CHALMERS

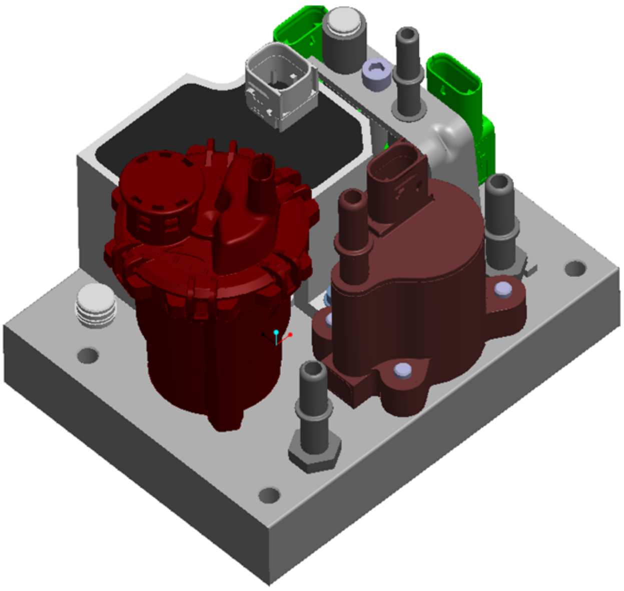

Master thesis

Modeling of a urea dosing system

Tobias Olsson

Automatic Control, Automation and Mechtronics
Department of Signals and Systems
CHALMERS UNIVERSITY OF TECHNOLOGY

EX005/2014

Abstract

In spring 2013, a new EU directive which further reduced the limits on harmful gases such as trucks may emit. Nitrogen oxides are one of the gases that are influenced by the new directive. It is therefore necessary that systems that reduces nitrogen oxides needs to be improved, one of those systems is called urea dosing system. As the improved urea dosing system is complex and difficult to debug it helps to have a mathematical model of the system. The thesis purpose is to create such model, the model can be used to see how the dynamics of the system is changed due too variations in hardware and for changes in the software. The system is assumed to be leak-free and the modeling focuses on doing a good model of the air subsystem. The verification of the system shows that the model correspond well to reality when ideal conditions are assumed, resulting in a low deviation. The model also manage a disturbance added to the input signal at least as good as the real system. The models created are also verified against how the system works in different temperatures and variations in hardware.

Keywords: **Trucks, Urea, UDS, Modeling, Pressure relief valve, Fluid flow, Simulink**

Sammanfattning

Våren 2013 introducerades ett nytt EU direktiv som ytterligare sänkte gränserna på farliga gaser som lastbilar får släppa ut. Kväveoxider var en utav de gaser som påverkades av det nya direktivet, ett av systemen som minskar kväveoxider kallas för urea dosering system och behövs således förbättras. Då det förbättrade urea doserings systemet är komplext och svårt att felsöka underlättar det att ha en matematisk modell av systemet. Denna rapports syfte är att skapa en sådan modell, modellen som skapas skall användas för att se hur systemets dynamik ändras vid variationer i hårdvaran, samt att ändringar i mjukvaran skall kunna testas och verifieras. Systemet antas vara läckfritt och modelleringen fokuseras på att göra en bra model av luft delsystemet. Verifieringen av systemet visar på att modellen motsvarar verkligheten väl då idealiska förhållanden antas, dessa tester gav låga avvikelse. Modellen klarar även av störningar på insignalen minst lika bra som det verkliga systemet. Modellerna som skapades testas även mot hur systemet fungerar vid olika temperaturer samt variationer i hårdvaran.

Keywords: **Lastbilar, Urea, UDS, Modellering, Övertrycksventil, Vätskeflöde, Simulink**

Acknowledgments

I would like to thank my supervisor Jonas Fredriksson at Chalmers who took the time to help me when I had problems in my simulations or to help me understand difficult parts of the model. I would also like to thank my co-workers at Volvo who encourage me when it was the hardest and especially my supervisor at Volvo Daniel Ireståhl. Who took the time to help me understand the real system, set it up for laboratory test and measurements. I would also like to thank my examiner Magnus Andrén at Volvo who had the understanding of that problem could occur during the thesis and the need to modify the work thereafter. Last but not least I would like to thank Matilda Rosander for her help with proofreading and giving feedback on the written report.

Göteborg, March 31, 2015

Tobias Olsson

CONTENTS

Nomenclature

β_a Effective bulk modulus for air

λ Flux linkage between the coil and plunger

μ Permeability of the plunger

μ_0 Permeability of free space

μ_p Permeability of the plunger

ρ_a The density of air that flows through the air valve

$\rho_{anozzle}$ The density of air which flows through the air nozzle

ρ_c The air density which flows through the pressure relief valve

θ_c The angle of the poppet closing the pressure relief valve

θ_a The angle of the plunger closing the air valve

a Length of iron through which flux passes

A_c The cross-sectional area of control volume 1

A_s cross-sectional area of the solenoid

$A_{anozzle}$ The discharge area for air nozzle

A_{dc} Discharge area for pressure relief valve

c The distance between plunger and solenoid

$C_{danozzle}$ Discharge coefficient of air nozzle

C_{da} Discharge coefficient for the air valve

C_{dc} Discharge coefficient for pressure relief valve

d The inner diameter of the air valves guide tube

D_c Cross-sectional diameter of control volume 1 for the pressure relief valve.

D_a Cross-sectional diameter of control volume 1

f The frequency of the PWM signal

F_c The Coulombs friction force

F_f The fluid's force

F_g	The gravitational force
F_s	The spring force
F_{diff}	The Coulombs friction's force
F_{mag}	Electromagnetic force that is acting on the plunger
F_{sf}	The steady flow force
F'_{sp}	The preload force on the spring
F_{uf}	The unsteady flow force
g	The gravitational constant
i	Current that drive the coil
I_s	Measured maximum current that is given to the solenoid
k_c	Spring constant for the spring acting in the pressure relief
k_a	The spring constant of the spring acting on the plunger
l	Length of the solenoid
$L(x)$	Inductance produced by the coil
L_c	The length of control volume 1 for the pressure relief valve
L_a	Length of control volume 1 for the air valve
M	Molar mass for the gas
m_c	The poppet's mass
m_p	The plunger's mass
N	Number of turn on the solenoid
P_c	The desired cracking pressure for the pressure relief valve
P_{atm}	The atmospheric pressure
P_a	Pressure in the air canal
P_{diff}	The pressure hysteresis for when the poppet is displaced
P_e	Pressure in the muffler (assumed to be equal to atmospheric pressure)
P_i	The inlet pressure to the air valve
P_{ma}	Mean pressure over the air nozzle
P_u	Pressure in the urea canal

Q_a The air flow into the air canal

Q_c The air flow through the pressure relief valve

$Q_{anozzle}$ Air flow through air nozzle

Q_c Flow through the pressure relief valve

$Q_{unozzle}$ Air flow through urea nozzle

R Gas constant

R' Total reluctance of the plunger

$R_{specific}$ Gas constant for air

T Absolute temperature of the gas

V_a The pressure sensing volume in the air canal

V_p Peak voltage that the power unit can deliver

V_u The pressure sensing volume in the urea canal

$W'(i, x)$ Co-energy

x Displacement of the plunger

x_0 The preload distance of the spring acting on the plunger

y The poppet's position

1 Introduction

This chapter will give a brief background to the problem discussed in the thesis. The chapter will then continue with a purpose, constraints and goal of the thesis. Lastly the procedure of the thesis is explained and ended with an outline describing the structure of this thesis.

1.1 Background

Nitric oxide (NO) is a colorless and odorless gas which can be synthesized in a laboratory from nitrogen and oxygen at high pressure and temperature. Nitrogen dioxide (NO_2) however has a red-brown color with an irritating odor. The gas is extremely reactive and is part of emission control catalysts to reduce among others carbon monoxide (CO) and diesel particulates through oxidation, as described in [1]. NO_2 is in high concentrations toxic to humans and can result in inflammation on airways. Further is NO_2 a contributer to formation of secondary particulate aerosols and tropospheric ozone (O_3) in the atmosphere. NO and NO_2 are often lumped together and called Nitrogen oxides (NO_x), NO_x is also a contributer to acid deposition and eutrophication. NO_x is therefore a negative performer on human health both direct and indirect. The largest contributer to NO_x emissions is by far combustion of fossil fluids where transport sector 2013 contributed with 40.5% according to European Environment Agency, [2].

From the transport sector it is mainly diesel engines exhaust that contributes with NO_x. This is due to the fact that diesel fuel consist of 75% Nitrogen, see [3]. NO_x emissions does not only depend on the amount of nitrogen in fuel but also on the air-fuel mixture and at what temperature the reaction is done, higher temperature usually means a higher ratio of NO_x in the emissions, see [2].

Those are the contributers to why nitrogen oxides from diesel engines has in European Union been regulated through directives beginning with Euro I, which was introduced 1992, [4]. With each new directive the allowed emissions has been narrowed down and todays active Euro VI directive has the hardest limits to achieve yet. It is not only NO_x which is regulated but also carbon oxide (CO) and particular matter (PM) to name a few. Similar directives exist outside the EU as well and a reason that the directives are not equal are due to the tests that are used to measure the exhaust are different. How the US and the EU directives for PM and NO_x has progressed during each new directives is seen in figure 1.1.

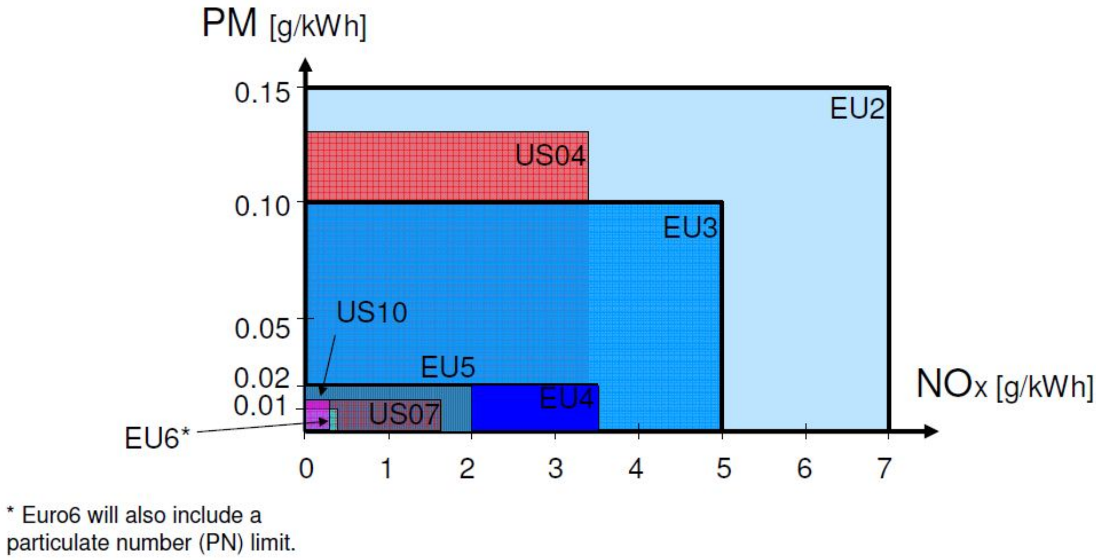

Figure 1.1. How USs and EUs emissions directives corresponds to each other, note that due to different verification driving cycles the two is not directly comparable.

The directives has been a driving reason to why truck manufactures has gone from no treatment of the exhaust gases to the advanced system they have today. Another driving factor to the development is that it is considered as a marketing method to have the most environmental friendly truck on the market. The latter factor gains ground as the buyers environmental thinking increases. The exhaust aftertreatment system often referred to as EATS consist of multiple system, everything from passive filter to catch soot to actively inject reducing agents into the system. Most of the subsystems is placed within the muffler on vehicle, and in this case a truck.

1.1.1 Exhaust aftertreatment system

A truck muffler is a piece of high technology that consist of multiple subsystems, which main purpose is to cleanse the engine exhaust gases. Each subsystem has its designated emission to reduce/transform through different chemical reactions with or without an injected reducing agent. This system will transform many of the toxic and greenhouse gases into harmless ones except for carbon dioxide (CO_2), see[5], a simplified schematic over a truck muffler and its EATS is shown in figure 1.2.

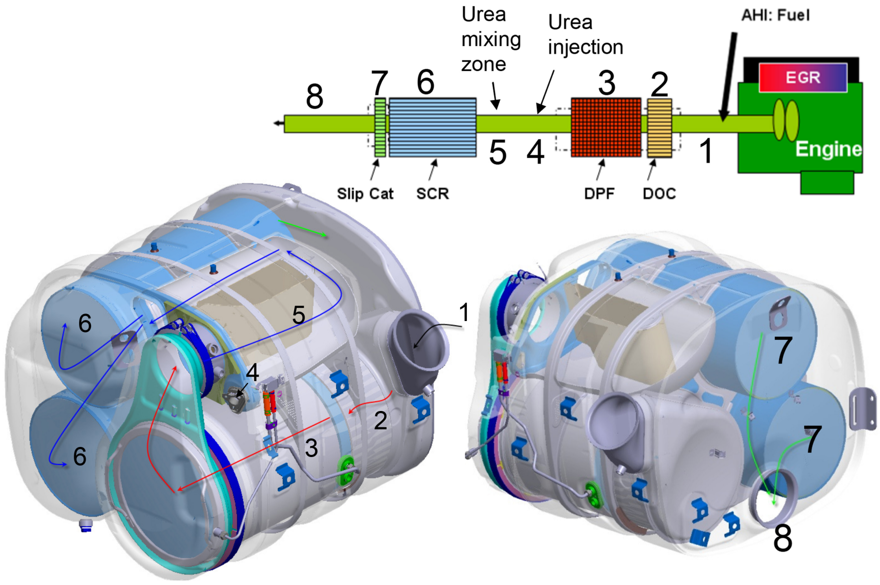

Figure 1.2. An overview of how the EATS works, in the top is there a simplified view of where the subsystems act related to each other. In the bottom is there a schematic view of the muffler and where the different subsystem act related to the muffler. The number corresponds to each other, [5].

The EATS is a work in progress and thus it receives new subsystems and improvements to existing ones. This is to further increase its potency to achieve future regulations. The subsystems in figure 1.2 is briefly explained in the list below and the number in the figure corresponds to the numbers in the list.

EGR: Exhaust Gas Recirculation reduces the NO_x amount drastically through heat exchanger between hot exhaust gas and the fresh inlet air.

1. **AHI:** Aftertreatment Hydrocarbon Injector injects fuel which oxidize in the catalyst to form heat that is needed for soot oxidation of the filter.

2. **DOC:** Diesel Oxidation Catalyst oxides hydrocarbon (HC) and CO from the engine into water (H_2O).

3. **DPF:** Diesel Particulate Filter collects PM, soot and ashes.

4. **Urea injection:** Urea Dosing System, injects urea-water solution into the exhaust, a more detailed description is given in chapter 2.

5. **Urea mixing zone:** The injected urea-water solution evaporates and mixes with the exhaust gases.

6. **SCR:** Selective Catalytic Reduction reduces NO_x into N_2, O_2 and H_2O using ammonia (NH_3) injected from the UDS.

7. **Slip Cat:** Oxidizes remaining ammonia from SCR.

This is a brief introduction to which subsystems a truck muffler consist of to purifying the exhaust. Urea dosing system (UDS), which this thesis is focusing on is describe in more detail in chapter 2.

1.2 Purpose

The aim of this thesis is to first do a study to get an understanding of how large percentage of fault codes in the urea control module that is faulty raised. Then make a model of the air subsystem of the system that later can be integrated with a model of the urea subsystem. The purpose of the integrated model is to locate the causes of fault codes in a simulation environment instead of locating it on a real installation. It will also be able to foresee how the system behaves if a physical parameter is changed.

1.2.1 Constraints

As the UDS is complex and the number of fault codes which are faulty raised this thesis can easily grow too large. To prevent this the following constraints need to be considered:

- only UDS for Euro VI type engines.
- only regard fault codes raised in the urea control module that is related to urea dosing system.
- only the newest main software of the urea control module.
- only the air subsystem will be modeled, due to the complexity of the UDS pump.
- no air flow loss inside the system.
- the modulated system will take inputs that are given by existing software.

1.3 Goals for the model

To verify that the model is good enough, simulation result will be compared with measurement data. The goals are that the model shall not deviate from the real system at steady state more than 10% at flow in/out and pressure at urea and air subsystem. The system shall also manage input disturbances equally good as the real system.

1.4 Procedure

This thesis is divided into two preliminary issues; extract and examine data to determine the diagnosed trouble code (DTC) frequency and also setup a model to simulate the UDS.

To determine the frequency of different DTCs and which are over representative among trucks, will be done by study data that has been collected from commercial trucks. The data is sent regularly either by a physical read out at a workshop, or the truck sends it directly to a database wirelessly. The latter is the most common one for newer trucks and as the data extracted is not depending on when the truck is at a workshop, the readouts are more regular. The data is sent and stored in bags to minimize the data size of each readout, a bag contains multiple data but no timeline i.e. you can see how far the truck has gone but not when this particular distance has been traveled. For crucial data such as when a DTC is raised or date when the truck is first put into traffic a timestamp is stored, see [6].

The data is stored in a database which can be accessed through either a manual readout or by a web interface. The first is preferred when large data extraction from the database is made, however it needs a good insight not only in how the database works but also in what its definitions corresponds too. A benefit is that the data extracted can be arbitrarily big and custom-made to contain exactly all the data that is necessary. The second option is built with the end-user in mind and is therefore vastly more user friendly with the drawback that it has restrictions, for example on how large datapool the search can result in. The data in this thesis is retrieved using the web interface as it is large enough to get a sufficient background to establish the DTCs frequency.

The second stage begins with electing a few of the more common DTCs to examine them further. One of those DTC is then elected for a thorough investigation with the goal of establishing the root cause i.e. what has triggered the software to invoke the DTC. From here a mathematical model of the relevant parts of the system are made either by the use of physics of first principle, by system identification or a mix of them. What method that is used is decided by the complexity of the system, number of needed parameters/unknowns and what that can be neglected. The model is then used to simulate how the system behaves in different scenarios and how the dynamics of the system would change if a physical parameter is changed.

1.5 Outline

The structure of this thesis is that in the next chapter the system that will be modeled is introduced and explained in detailed, to give an understanding of the complexity of the system. Followed by the study of DTCs that occurs in the aftertreatment control module (ACM) including a brief root cause analysis of the selected DTC. The study will be followed by the modeling chapter where each part of the real system is modeled separately. The models are in the next chapter simulated and compared against measurements from the real system, to see if the goals are achieved or not. The thesis ends with a discussion of choices that has been made during the work and a short chapter conclude the thesis and present potential future work.

2 Urea dosing system

This chapter will in detail describe the system that this thesis focus on. First it will give an explanation of the purpose of the system and then continue with describing the parts which the system consists of.

2.1 Urea dosing system

The UDS sprays a urea-water solution ($\approx 32.5\%$ weight of urea) often referred to as UWS or by its commercial name AdBlue through atomization into the muffler, see [7]. Subsequently the reducing agent NH_3 is generated by evaporation of water, thermolysis of urea and hydrolysis of isocyanic acid. However this is not trouble-free, due to the inertia of the droplets and the slow thermolysis and evaporation of them, a wall film can arise on the muffler's wall. This film will decrease the temperature which leads to a slower rate of evaporation of the UWS which increase the risk of melamine complexes arises from the urea solution. If melamine complexes forms, the NH_3 generated is drastically decreased which subsequently lower the amount of NO_x that can be reduced in the SCR. It is therefore important to inject the UWS according to how much NO_x there is in the muffler, its temperature and to keep the spray at an optimized atomization of the liquid, as described in [7]. Another problem is that UWS has a freezing point at -11° C but trucks is required to be fully operational down to -40° C. This problem is solved by heating the UWS tank and its hoses. To prevent the UWS to freeze when the truck is off, air enters the urea canal to purge it from UWS at key off.

Some truck manufacturers introduced recently a new version of UDS consisting of completely new hardware and software to meet the new regulations in the European Union which was taken into effect in January 2013 (EURO VI) [4]. Although the system has nearly two years in the market there are parts of it that still needs to be investigated further to increase the understanding of the whole system. The DTCs are treated individually depending on how important that specific DTC is. If a crucial DTC has been raised during a few successive tests the truck receive a limit on the engine speed until it has been served. This makes it inconvenient for the driver and truck manufactures to raise DTC even if the system works properly, [6].

2.2 System description on UDS

The UDS system consist of five parts; pump unit (PU), dosing nozzle (DN), ACM, UWS tank, hoses and the electrical main software (EMS). The EMS is not an active part in the UDS as it only collects DTCs thats have been invoked in the ACM and make the corresponding adjustments to the truck. How they are connected to each other is shown in the schematic figure 2.1.

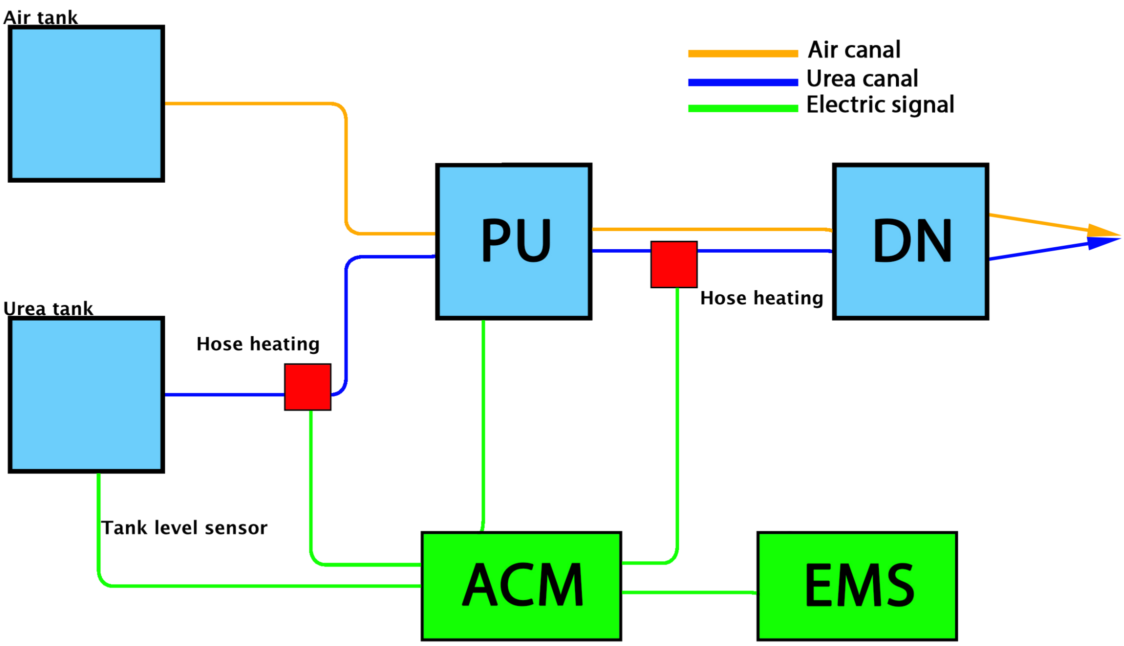

Figure 2.1. A simple schematic over the UDSs parts and how they are connected to each other.

There exist different version and appearances of the dosing nozzle to match the variety of work conditions they are exposed to, a common version of the dosing nozzle can be seen in figure 2.2. The dosing nozzle is a static mechanical part and can therefore not change its characteristics, there is however a small variation among the nozzles due to variation when manufactured. The UWS and air is mixed together the moment they leave the nozzle.

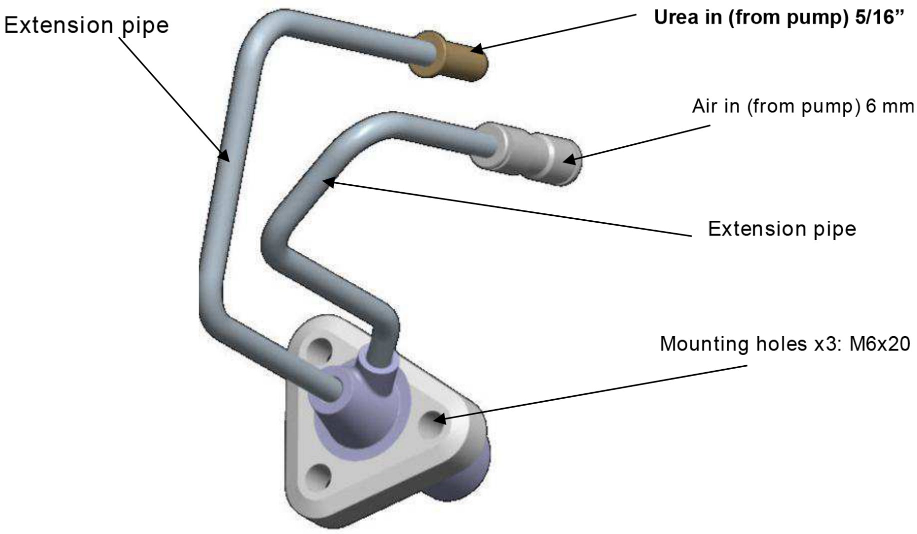

Figure 2.2. A picture to show the dosing nozzle and its parts, [8].

The PU consist of several actuators and sensors which are used to optimize the amount of UWS, which is injected into the exhaust gas. A picture of the PU is seen in figure 2.3 showing the parts for air, UWS and coolant liquid. The UWS amount that is injected is controlled by varying the frequency of the pump, the ureapump can work in frequencies from 0.25 Hz up to 58 Hz. The air flow is controlled by an air control valve on the PU to have an optimal atomization in the dosing nozzle at different dosing amounts.

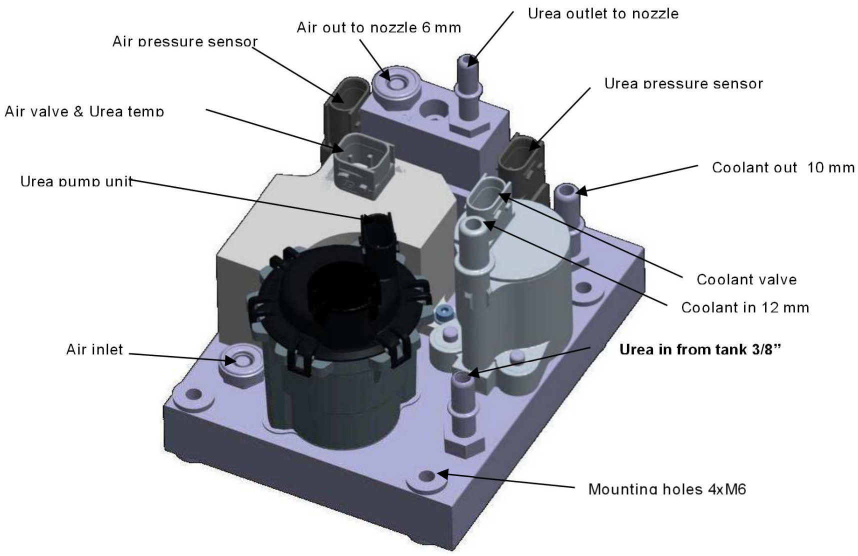

Figure 2.3. A picture of the pump unit used in this thesis displaying inputs and sensors, [8].

3 Study of DTC frequency

This chapter will present a preliminary study of how frequent different DTCs are invoked within the ACM, the data is extracted from the database using the web interface. Then one of the predominantly DTC is selected for an investigation of what could have caused the DTC to be raised.

Due to confidentiality reasons this chapter has been partly censored. That is the reason to why the DTCs name has been censored along with the values on the axis in the bargraphs.

3.1 DTCs frequency

The data that will be presented here is collected over three months from first of June 2014 until last of August 2014. The collection consist of 10695 vehicles where 3900 is using the latest main software (MSW). During this time, DTCs where invoked in the latest MSW and a few more in grand total. In the bargraph in figure 3.1 the top 4 DTCs is represented.

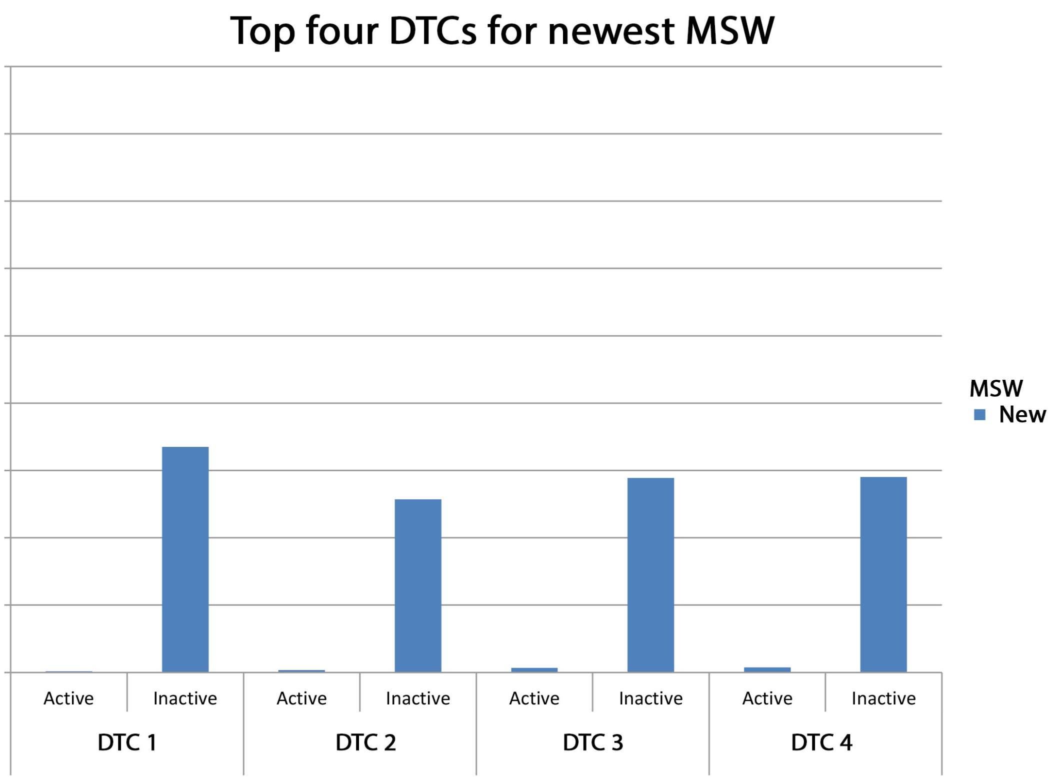

Figure 3.1. Top four DTCs during June to August that is invoked from a vehicle that is using the newest MSW

The four DTCs makes an equally large impact to the number of encountered DTCs, with "DTC 1" providing a slightly larger impact than the other three. The status inactive or active indicates whether the DTC is active now (active) or if it has been active and then in someway repaired itself without doing a maintenance (inactive). It is highly possible that DTCs which have many inactive errors suffer from error in calibration or that the limits which the values are checked against are not optimized correctly. Further it is not enough just to know which DTC that has the highest frequency since a few vehicles may account for nearly all of the occurrences displayed in figure 3.1. It is therefore necessary to include an additional graph that display how many unique vehicles which has invoked a DTC, this is shown in figure 3.2.

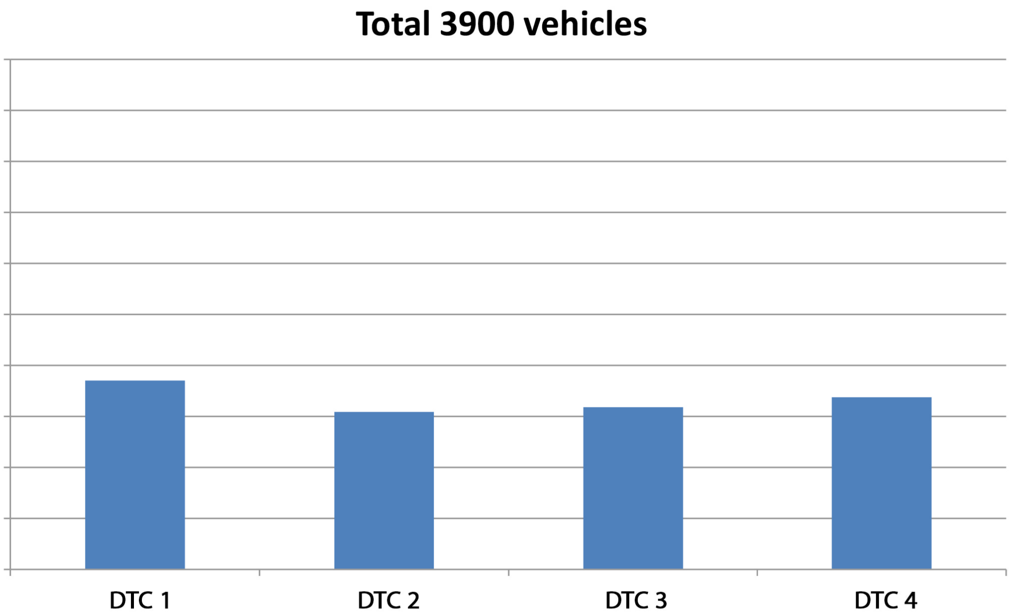

Figure 3.2. Number of unique vehicles that have a specific DTC, note that one vehicle can occur on several DTCs.

From the figure above it can be concluded that there is no DTC that affect significantly more vehicles than the others.

3.2 Selection of DTC

The DTC that will be chosen for further studies is "DTC 4". This is due to the fact that it is a major contributor of DTCs in the ACM and is found in many vehicles. Further the DTC was found with the on board diagnostic and is of a mechanical error type. The DTC can be simulated through mathematical modeling. In comparison with "DTC 1" or "DTC 3" where the first is a communication problem between two control modules in the vehicle and the latter is a DTC which is sent to the

ACM from an external part on the vehicle which means that the problem does not necessary has to be within the PU. The reason to why "DTC 4" is chosen instead of "DTC 2", is that "DTC 2" are more extensive and comprises more parts and the solution to the DTC might not even be within the UDS.

When a DTC has occurred it is stored in the vehicle along with data, such as the time it occurred and a compositional key for that specific DTC. The key contains data of which part that has failed and how that part has failed. This information can give a hunch of what might have invoked the DTC and where to look for a solution. The reason why this specific DTC was invoked is shown in figure 3.3, the figure shows the total number of occurrences for the latest two MSWs. The second newest MSW is included in the figure to see whether the newest MSW reduce/increase or does not affect the number of invoked DTCs at all.

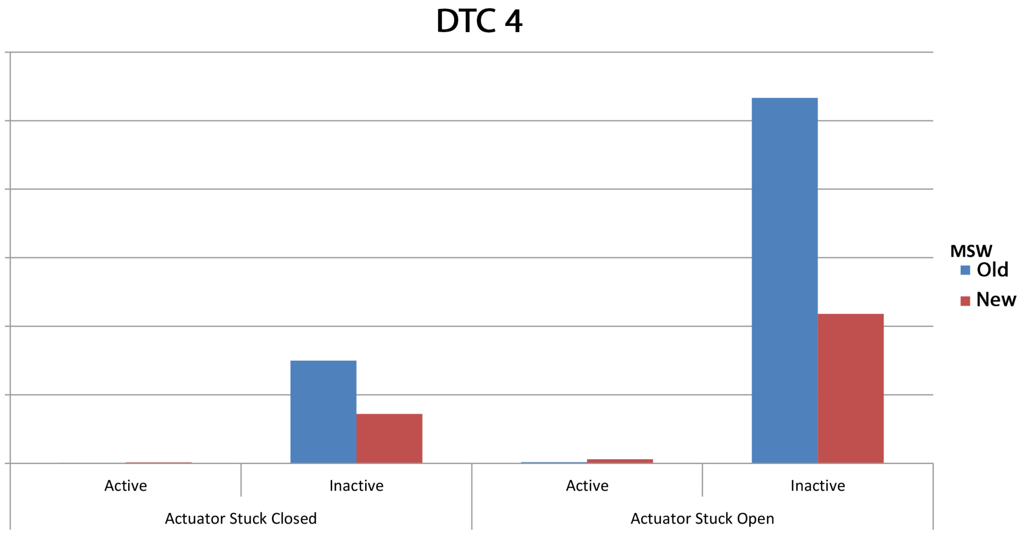

Figure 3.3. The reason why "DTC 4" has been invoked on the two latest MSWs

As the figure shows the newest MSW has decreased the number of occurrences drastically. This indicates that this is not completely an hardware problem but a software problem as well and that it is still not fully optimized.

As seen in this chapter the invoked DTCs are mainly from the air subsystem and the chosen DTC is related to the air subsystem as well. To get the most out of the model, the air subsystem will be modeled. The modeling is described thoroughly in chapter .

4 Modeling

This chapter will derive a mathematical model of the system, to make it more comprehensible, the complete system will be divided into smaller parts beginning with the most fundamental one. The fundamental fluid mechanics assumptions Conversation of Mass, Conservation of Momentum and Conservation of Energy within the system will be used if nothing else is mentioned, see [9] and [10]. Along with those the continuum hypothesis will also be used, it basically states that even though a fluid consist of millions of particles it can be treated as they where all in continuum in small regions, a more thorough definition is found in [11]. Those assumptions is used both due to it is widely use in fluid mechanics and as they are suitable for this modeling. Figure 4.1 give an overview of the system to facilitate understanding of what will be modeled. The coolant canal and the urea pump will not be modeled as they is outside the scope of this thesis.

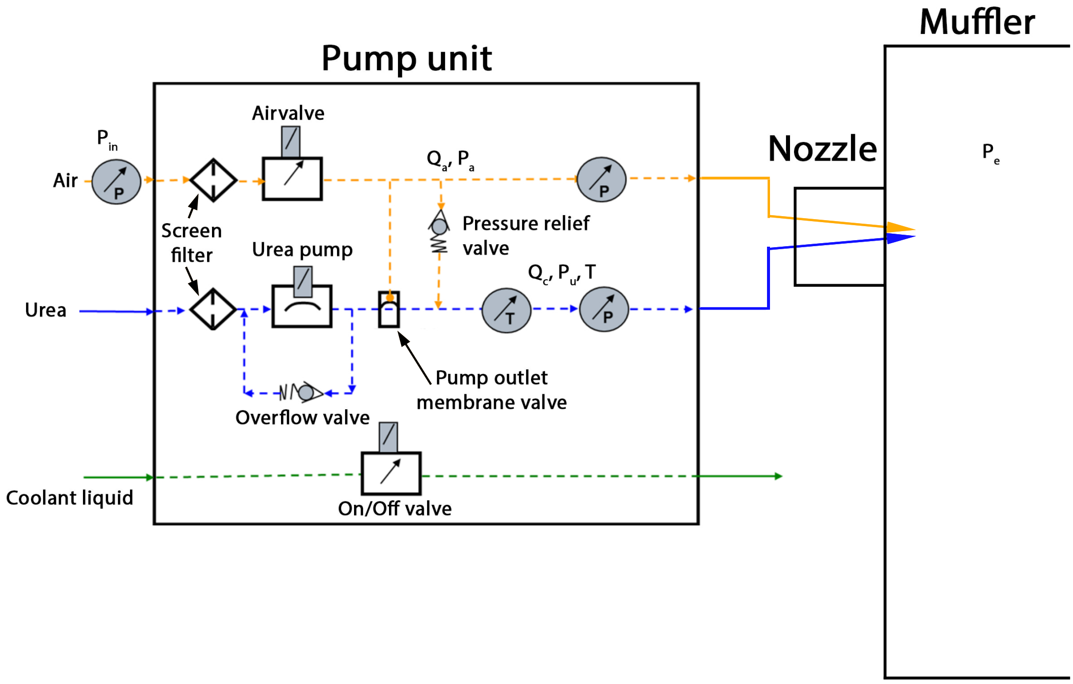

Figure 4.1. A visualization of which part that is to be modeled and how the interact with each other, [12].

In the beginning of this thesis it was stated that the modeling should be either physical, system identification or a combination of them both. The modeling presented in this chapter consist solely of physical modeling. The reason for only using physical modeling is that the parts that will be modeled is simple enough and consists of only one mechanical part for each model. It is also preferable to use physical insight to capture the dynamics of each acting force and the dynamics of the whole system.

So e.g. if the spring coefficient would change for some reason the model could be tuned accordingly.

4.1 Urea and air nozzle

The first part to be modeled is the nozzle, it is a fixed mechanical part which means that it does not contain any parts changing over time thus it is only depending on pressure in each canal. Since the dynamics between the two orifices is equal but independent of each other only the air nozzle will be described. A schematic view of the nozzle displaying all parameters used to model the nozzle is shown in figure 4.2.

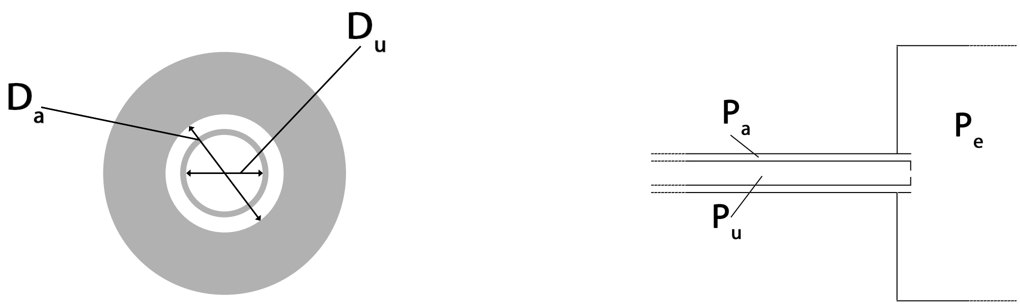

Figure 4.2. To the left the orifice is shown and the one to the right is an overview over the nozzle and the muffler.

This model begins with the equation of flow through an orifice which has been derived in previous literature, see e.g. [13] [14], as:

$$Q_{anozzle} = C_{danozzle} A_{anozzle} \sqrt{\frac{2(P_a - P_e)}{\rho_{anozzle}}} \tag{4.1}$$

where $Q_{anozzle}$ is the volumetric flow through the air nozzle. P_a and P_e are the pressure in the air canal and in the muffler respectively. $A_{anozzle}$ is the discharge area of the air orifice on the nozzle calculated with basic geometric equation for a circle and $C_{danozzle}$ is a design parameter that is called discharge coefficient. Due to the mufflers large volume, P_e is assumed to be constant at atmospheric pressure. The atmospheric pressure is for simplicity reason set to be equal to zero. However, P_a change with time which causes the density of the fluid to change over time as well. Therefore density has to be derived using the ideal gas law, [15], as:

$$\rho_{anozzle} = \frac{MP_{ma}}{RT} \tag{4.2}$$

where $\rho_{anozzle}$ is the density of air flowing through the air nozzle. T is the absolute temperature of the gas in Kelvin. The temperature is assumed to be constant over the whole system and time invariant. P_{ma} is the mean absolute pressure over the nozzle, M is the molar mass and R is the gas constant and both is specific for different ideal gases. The ideal gas law is not direct applicable as air is not an ideal gas, this is solved by using an specific gas constant that has been predetermined for air:

$$R_{specific} = \frac{R}{M} = 287.058 \tag{4.3}$$

The mean absolute pressure over the nozzle is computed with:

$$P_{ma} = \frac{P_a + P_e}{2} + P_{atm} \tag{4.4}$$

the P_{atm} that is added to the mean pressure is to compensate for that all pressures in the modeling use atmospheric pressure as zero, instead of absolute pressure as zero. Substitute (4.3) and (4.4) into (4.2) gives an expression for the density.

$$\rho_{anozzle} = \frac{P_a + P_e + 2 * P_{atm}}{2R_{specific}T} \tag{4.5}$$

The complete nozzle flow model is based on two governing equations, the equation of flow through an orifice (4.1) and the equation for how density vary with respect to pressure (4.5).

4.2 Pressure relief valve

The next part to be modeled is the pressure relief valve which separate the air and urea canal when the pressure in the air canal is below a desired cracking pressure. Occasionally the pressure will rise above the cracking pressure and thus opens the pressure relief valve. A picture of the component is seen in figure 4.3. The model is derived from the flow equation through an orifice, the orifice area depends on the displacement of the poppet valve which is in turn depended on the pressure difference between inlet and outlet. The derivation begins from the simplified schematics over the pressure relief valve shown in figure 4.4.

Figure 4.3. The pressure relief valve that is used in this thesis.

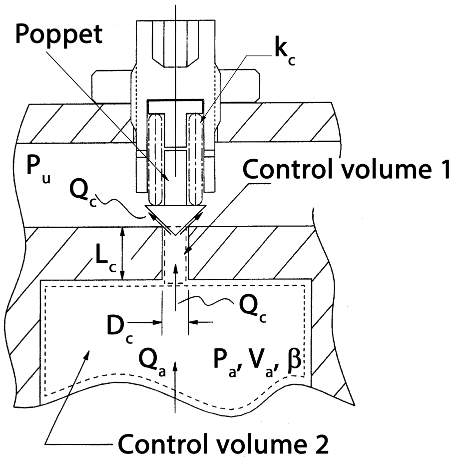

Figure 4.4. This shows the definitions of the physical quantities and the control volumes that are used to derive the mathematical model, [16].

The fluid in control volume 1 is assumed to be incompressible, and therefore the flow into the volume has to be equal to the flow out of it which is represented by the variable Q_c. It is the fluid forces from control volume 1 that is acting on the poppet to displace it in positive y direction while the spring tries to counteract the fluid forces. Control volume 2 has a fixed volume much greater than control volume 1 and the fluid inside it is assumed to be compressible with a modulus of elasticity given by β_a. The flow into control volume 2 is labeled, Q_a, and the pressure is named P_a as control volume 2 also is the air canal. The pressure in the exhaust chamber is defined by the variable P_u as the exhaust chamber in this case is the urea canal.

The flow and density equations are the same as those used to model the nozzle, except for how the variables are labeled. The equation for flow is found in (4.1) and the equation for density is found in (4.5). The equation with the variables labeled correctly for the pressure relief valve is found below:

$$Q_c = C_{dc} A_{dc} \sqrt{\frac{2(P_a - P_u)}{\rho_c}} \tag{4.6}$$

$$\rho_c = \frac{P_a + P_u + 2 * P_{atm}}{2 R_{specific} T} \tag{4.7}$$

here Q_c is the flow through the pressure relief valve. C_{dc} is the discharge coefficient and ρ_c is the density of the air flowing through the pressure relief valve. The discharge area A_{dc} for the pressure relive valve is not fixed but here it vary with the poppet position and increases with its displacement. The relation between A_{dc} and the poppet's position is described using the equation in [17] as:

$$A_{dc} = \pi y \sin\theta_c (D_c - y \sin\theta_c \cos\theta_c) \tag{4.8}$$

where θ_c is the angle of the poppet. D_c is the cross-sectional diameter of control volume 1 and the position of the poppet is denoted with y. The relation between the poppet's position and the discharge area can be seen in figure 4.5. The position is equal to zero when the valve is closed and the position can be derived using Newton's second law of motion. It states that an objects mass times its absolute acceleration is equal to all forces acting on the object, see [16] and [17]. Using a free body diagram of the poppet shown in figure 4.5 all forces acting on the poppet was derived, resulting in:

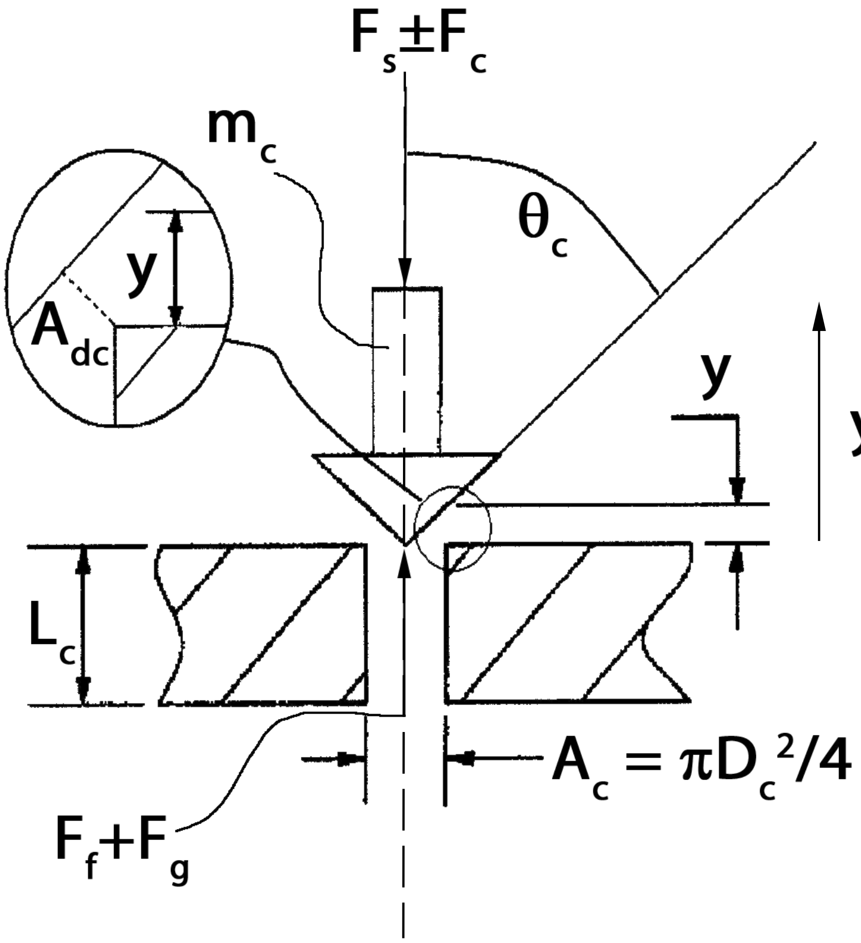

Figure 4.5. The free body diagram of the poppet and control volume 1, it also displays the relation between A_{dc} and y, [16].

$$m_c\ddot{y} = -F_s \pm F_c + F_f + F_g \tag{4.9}$$

where m_c is the mass of the poppet, $\ddot{y}$ is the acceleration of the poppet, F_s is the spring force, F_c is Coulombs friction and the fluid force from control volume 1 acting on the poppet is denoted with F_f. The spring force F_s can be divided into a conventional spring force and a preload force which must be exceeded before the poppet will begin to be pushed inwards, this is known as desired cracking pressure P_c. Using the definition of spring preload as defined in [16] gives the following expression for spring force:

$$F_s = k_c y + F'_{sp} = k_c y + A_c P_c \tag{4.10}$$

where k_c is the spring constant and A_c is the cross-sectional area of control volume 1. P_c is the cracking pressure for the valve i.e for what pressure in control volume 1 that the pressure relief valve should begin to crack open which is given from the technical specification of the pressure relief valve.

Further the Coulombs friction is the force which gives the system a hysteresis as it applies a force in opposing direction of the poppet's velocity [17], given as:

$$F_c = F_{diff}(-sign(\dot{y})) = A_c P_{diff}(-sign(\dot{y})) \tag{4.11}$$

the F_{diff} is the intensity of Coulombs friction force and can be calculated from A_c times P_{diff}, where P_{diff} is the error margin of the cracking pressure where the pressure relief valve is allowed to operate. P_{diff} can be found in the technical specification of the pump unit. In this application the gravitational force is acting to open the poppet. The expression for gravitational force is well known and is given as:

$$F_g = m_c g \tag{4.12}$$

where g is the earth's gravitational acceleration. The last force which act on the poppet is the fluid force which itself consist of two parts, one steady state part and one transient part. Both parts has been derived in published literature, [17], as:

$$F_f = F_{sf} \pm F_{uf} \tag{4.13}$$

The steady state force applied by the fluid is seen below:

$$F_{sf} = A_c P_a \tag{4.14}$$

and it consists of the pressure from the fluid P_a multiplied with the area which the pressure is acting on A_c. The area is approximated to be equal to the cross-sectional area of control volume 1. The unsteady flow force equation is defined as:

$$F_{uf} = \pi \rho_c L_c C_{dc} \sin\theta_c \left((D_c - y\sin(2\theta_c)) \cdot \frac{dy}{dt} + \frac{y(D_c - 0.5y\sin(2\theta_c))}{\sqrt{2\rho_c(P_a - P_u)}} \cdot \frac{d(P_a - P_u)}{dt} \right) \tag{4.15}$$

which depends on $\dot{y}$ and the pressure change of difference between the pressure of control volume 2 and the exhaust chamber pressure. Here ρ_c is the fluid density over the pressure relief valve derived in (4.7), L_c is the length of control volume 1 and θ_c is the angle of the poppet. By substituting (4.10)-(4.15) into (4.9) a complete expression for the poppet's displacement is achieved.

The last part to make this model complete is an expression for pressure in the air canal, which is obtained from the pressure raise equation:

$$\dot{P}_a = \frac{\beta_a}{V_a} \left(Q_a - Q_c - Q_{anozzle} - A_c \frac{dy}{dt} \right) \tag{4.16}$$

where β_a is the effective bulk modulus for air in control volume 2. V_a is the volume of the air canal. The flow into the air canal and through pressure relief valve are known as Q_a and Q_c respectively.

The complete model of the pressure relief valve is obtained by substitute the expression for the discharge area equation (4.8) into (4.6). And the complete expression for the poppet's motion that is obtained by substituting (4.10)-(4.13) into (4.9) and the expression for pressure rise from (4.16).

However, it is not enough to only model the physical part of the pressure relief valve. It is also necessary to model the hard constraints on the poppet's end positions. As this introduces discontinuities to the model it is not modeled using physical equation but using a logical block in Simulink. This logical block can be see in figure B.3. The logical block checks if the plunger is in any end position and will reset the velocity of the plunger if the acceleration tries to force the plunger further in that direction. Along with this logical block the position integration is done by an integration limiter which will not integrate a position that is larger than the defined end positions. This logical block is later also used when the air valve is modeled.

4.3 Urea canal

So far the air and urea nozzle has been modeled to return a flow for a specific pressure. When modeled the pressure relief valve it gave a specific pressure in the air canal for a given inflow, this pressure is then used to calculate the flow through both the pressure relief valve and the air nozzle out. Next thing to model is that a given flow through the pressure relief valve gives a specific pressure in the urea canal. The model of pressure in the urea canal is trivial and the only thing needed is the pressure rise equation:

$$\dot{P}_u = \frac{\beta_a}{V_u}\left(Q_c - Q_{unozzle}\right) \tag{4.17}$$

where V_u is the volume of the urea side including hoses from the pump unit to the nozzle. Q_c and $Q_{unozzle}$ are the flow into urea side from the pressure relief valve and flow out of the urea canal through the urea nozzle respectively. The equation describe how the pressure will change depending on the flow into and out of the canal.

4.4 Model of air valve

The air valve is of a proportional solenoid valve type. A cross-sectional view of the solenoid and guide tube is seen in figure 4.6 and similarities with the pressure relief valve model can be drawn. This section will instead focus on determining the magnetic force induced by the solenoid and act on the plunger to open/close the valve, this force is time dependent with both displacement of the plunger and current into the coil. A schematic view of the air valve is seen in figure 4.7.

Figure 4.6. A cross-sectional view over the solenoid in the air valve.

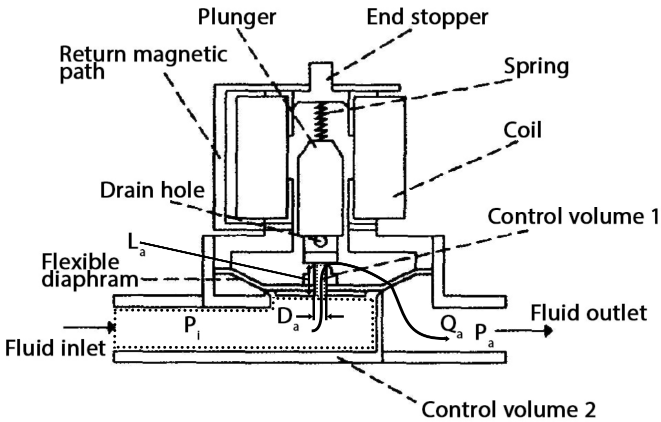

Figure 4.7. This shows the designation of the physical quantities and the control volumes that is used to derive the mathematical model, [18].

The pressure of control volume 2 is assumed constant, this is due to the large size of the volume and that it is constantly supplied with pressure by a compressor. This leads to that there is no need to approximate the pressure using a pressure rise equation. The flow through the air valve is assumed to be derived using the same equation as for the pressure relief valve and is expressed using equation:

$$Q_a = C_{da} A_{da} \sqrt{\frac{2(P_i - P_a)}{\rho_a}} \tag{4.18}$$

where

$$A_{da} = \pi x \sin\theta_a (D_a - x \sin\theta_a \cos\theta_a) \tag{4.19}$$

The displacement of the plunger is derived using Newton's second law of motion, the free body diagram of the plunger can be seen in figure 4.8, and is expressed as:

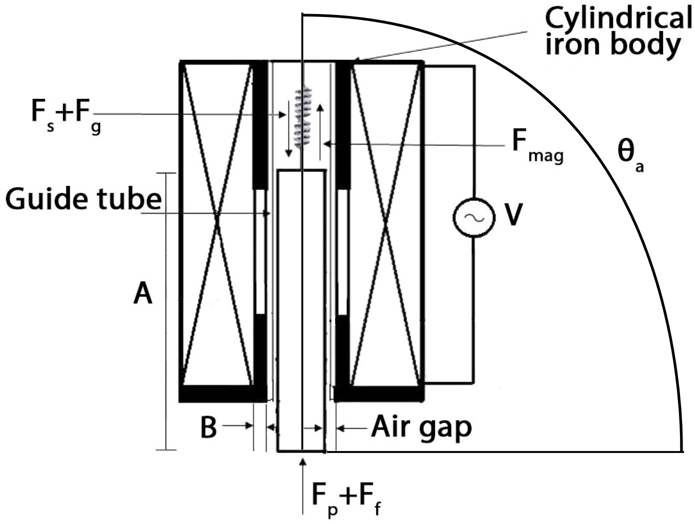

Figure 4.8. Free body diagram of the plunger in the air valve, [19].

$$m_p\ddot{x} = F_f + F_{mag} - F_g - F_s \tag{4.20}$$

The expression for magnetic force F_{mag} is describe in the next paragraph. The expression for fluid force F_f, gravitational force F_g and spring force F_s is derived in the same equation as for the pressure relief valve resulting in equations:

$$F_g = m_p g \tag{4.21}$$
$$F_s = k_a x + F'_{sp} = k_a x + k_a x_0 \tag{4.22}$$
$$F_f = F_{sf} \pm F_{uf} \tag{4.23}$$
$$F_{sf} = A_a P_i \tag{4.24}$$

$$F_{uf} = \pi \rho_a L_a C_{da} \sin\theta_a \left((D_a - x\sin(2\theta_a))\cdot \frac{dx}{dt} + \frac{x(D_a - 0.5x\sin(2\theta_a))}{\sqrt{2\rho_a(P_i - P_a)}} \cdot \frac{d(P_i - P_a)}{dt} \right) \tag{4.25}$$

The magnetic force F_{mag} induced by the solenoid has been derived in previous literature with different approaches. Either by approximating the flux linkage as a function of inductance and plunger displacement as in [19] and [20] or by curve fitting a flux linkage measured data to equations as in [18] and [21]. In this thesis the approximation of flux linkage to determine the magnetic force is used, [19]:

$$F_{mag} = \frac{\partial W'(i,x)}{\partial x} \tag{4.26}$$

where $W'(i,x)$ is the co-energy which can be estimated from the integration of linkage against current, as in [18]:

$$W'(i,x) = \int_0^i \lambda(i,x)di = \frac{1}{2}L(x)i^2 \tag{4.27}$$

$\lambda(i,x)$ is the flux linkage between the coil and the plunger and the current feed into the solenoid is denoted with i. The current is approximated from an alternative current (AC) into an average direct current (DC). $L(x)$ is the inductance produced by the coil, the inductance of the coil varies due to the variation in total reluctance which in turn depends on the variation on the upper gap due to the displacement of the plunger and can be approximated as:

$$L(x) = \frac{N^2}{R'} = \frac{\pi d \mu_0 \mu a N^2}{c} \left(\frac{x}{x+a} \right) \tag{4.28}$$

where N is number of turns in the coil, R' is the total reluctance of the coil, d is the inner diameter of the guide tube in which the plunger is sliding. μ_0 and μ_p is the permeability of free space and permeability of the plunger respectively, a is the length of the plunger through which flux passes and c which is the thickness of the guide tube i.e. from the inner part of the tube out to the inner start of the coil. By introducing the variable L' the equation above can be simplified into:

$$L(x) = L' \left(\frac{x}{x+a} \right) \text{where} \quad L' = \frac{\pi d \mu_0 \mu_p a N^2}{c} \tag{4.29}$$

The complete expression for the magnetic force is obtained by substituting (4.29) into (4.27):

$$F_{mag} = \frac{i^2}{2} \frac{aL'}{(a+x)^2} \tag{4.30}$$

However the number of turns in the coil N, of the solenoid is not known and has to be estimated through laboratory experiments and this is explained in appendix A.

The discontinuities that are introduced by the hard end positions of the plunger is solved using the same technique as for the pressure relief valve.

5 Simulation and Result

In this chapter the mathematical models derived in previous chapter will be simulated and compared with sampled data from the real application where such data exists. Due to few measuring points on the device, what can be measured and later compared, is limited to outlet and inlet air pressure, outlet urea pressure and temperature. The mass flow into and out from air canal will be measured and as the system is assumed to be a leakage free the flow out through the urea canal can be calculated from the inlet and outlet flow. The computation of urea outlet flow is valid as a flowmeter measuring mass flow is not affected by upstream pressure [22]. First the real system measured data will be presented to give a better understanding of how the system behaves and how it was tested.

Each verification section will begin with presenting parameter values which have been used in the simulations, this will be followed by a short description on how the model has been implemented in Simulink. The sections will end with a presentation of the simulation in form of plots where the simulated data will be compared with the real system. The comparison will be done at steady state of 158 kPa.

5.1 Measured real system

This section will present data that is sampled from a real system and it is later used to compare how well the simulation corresponds to the real system. To measure the flow through the system two test are performed one where the air inflow was measured and one where air outflow where measured. Each test where iterated ten times to investigate the repeatability of the system and to get a mean to minimize the impact of disturbances.

The tests are performed using a custom built program that connected to and sent commands to the ACM via its connection with the CAN sampling software ATI Vision. The tests are run without UWS in the system and the air valve dutycycle increased from 0% to 100% using steps of 5%, with smaller steps of 2% at the systems normal operation which is between 30% to 50%. Each step is measured for 20 seconds to capture both the transient of the switch and the steady state for that specific dutycycle.

A schematic view of the test setup is seen in figure 5.1, the figure show where in the system the measurements are made for the different tests. The flowmeter is placed before the system (position 1) for the first ten test and then placed after the system (position 2) for the last ten. As the flowmeter measuring in g/s it has to be recalculated using equation (4.5) to achieve a volumetric flow which then can be used to correlate with the simulations. All sensors are sampled at 1000 Hz which is the maximum frequency of the hardware.

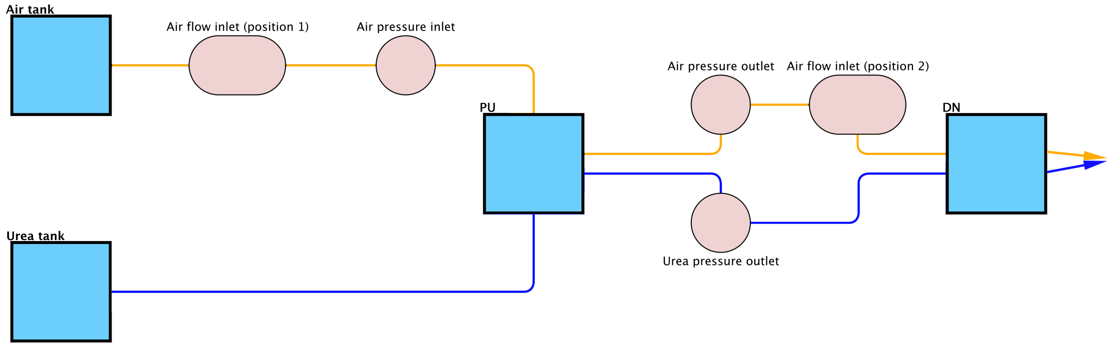

Figure 5.1. A schematic view of the test setup showing where the different pressures and flows where measured. Position 1 was where the flow was measured for the first ten tests and position 2 for the last ten.

Figure 5.2 shows the data collected on all tests where the inflow was measured, figure 5.3 on the other hand displays the ten tests where outflow was measured. The mean of those tests is later used to correlate how good the simulation corresponds to the real system.

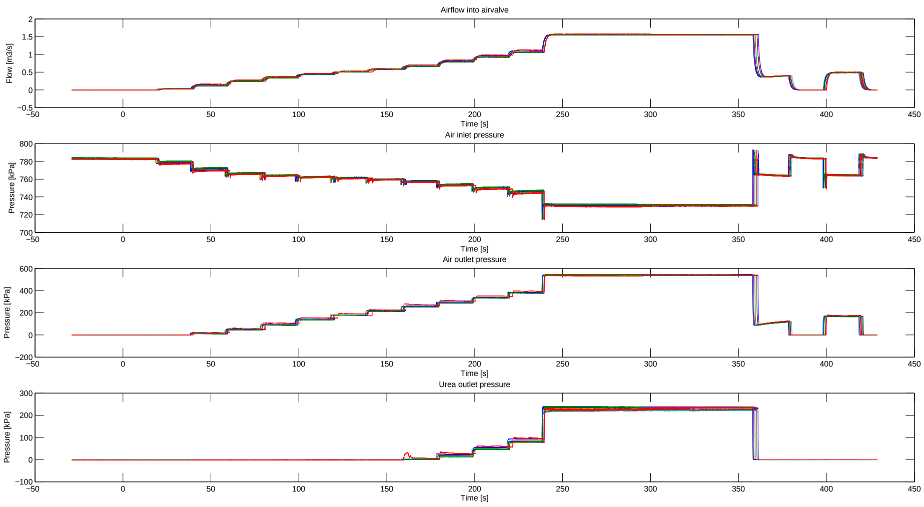

Figure 5.2. All measurements in same plot to show the correlation between the tests.

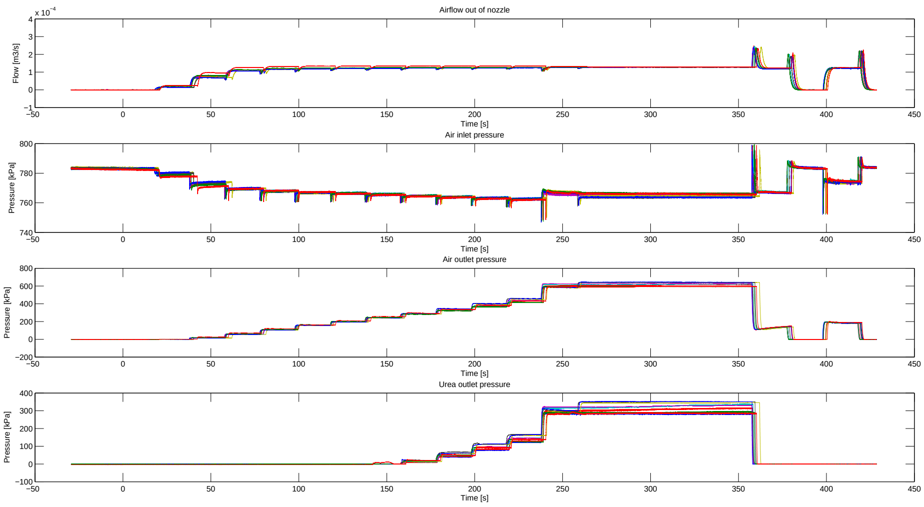

Figure 5.3. All measurements in the same plot to show the correlation between the tests.

The figures shows that the correlation between each test is high, which indicates good repeatability. This is needed to make a good theoretical approximation. Even though all test were performed exactly the same, there is a difference between the system pressures P_a when the inlet flow versus when the outlet flow is measured. This pressure difference arise from the flowmeter and where it is positioned as it is the only difference between the two test setups. This means that the flowmeter is not ideal and induce a pressure drop to the system that increase with inlet flow rate and upstream pressure. If the air inlet pressure is compared from the two test setups it can be concluded that the inlet air pressure when measuring the inlet flow is decreased more than when the outlet flow is measured this is due to the pressure drop in the flowmeter. Also the air inlet pressure for the last tests are increased when the air valve opens up maximum which is also caused by the pressure drop induced by the flowmeter. Assuming no leakage in the system, gives that the urea flow can be computed as the difference between air inflow and outflow which is shown in figure 5.4.

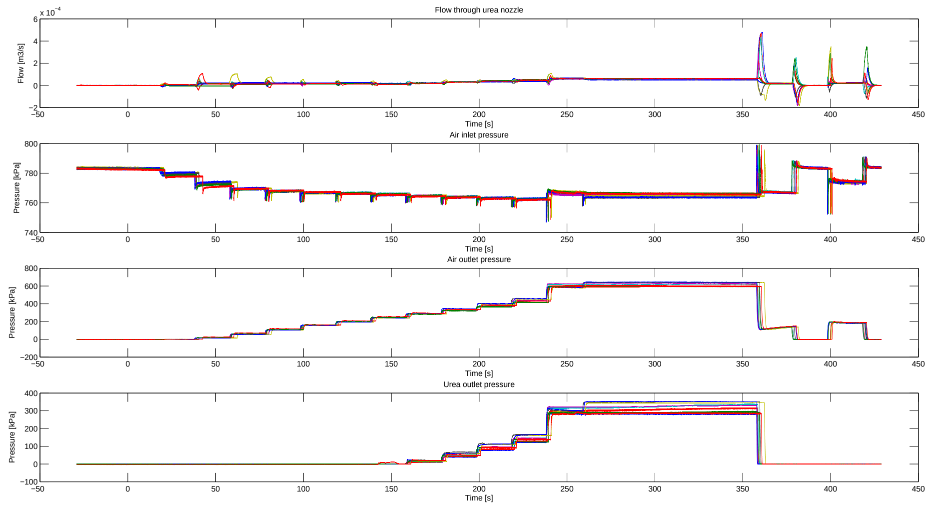

Figure 5.4. The air flow through the pressure relief valve and out through the urea nozzle. Note there should not be any pressure in the urea canal until air pressure rise above 260 kPa.

It is seen from the figure that the assumption that there is no leakage in the system does not hold. It is disproved as there is a flow out through the urea canal even as there is no pressure. There might be some minor error in the flow as it is computed indirectly from the inlet and outlet flow where there is a slight difference in pressure. However, is the pressure difference between the two tests too small to create such inaccuracy of flow in the urea canal. According to [22] a flowmeter measuring mass flow will in theory be unaffected for different pressures giving the conclusion that there is leakage within the system.

5.2 Simulation and verification of air nozzle

The air nozzle has a few physical parameters that are derived from measuring. The design parameter $C_{danozzle}$ along with the physical parameter values are shown in table 5.1.

Table 5.1. Fixed geometry parameters for air nozzle

Symbol	Description	Value	Units
D_u	Outer diameter of urea orifice	1.6	mm
D_a	Outer diameter of air orifice	1.75	mm
T	Absolute temperature of the fluid	295	K
$R_{specific}$	Gas constant for air	287.058	J/Kg K
$C_{danozzle}$	Discharge coefficient	1.15	n/a

The implemented Simulink model of the mathematical model derived in section 4.1 is seen in figure 5.5.

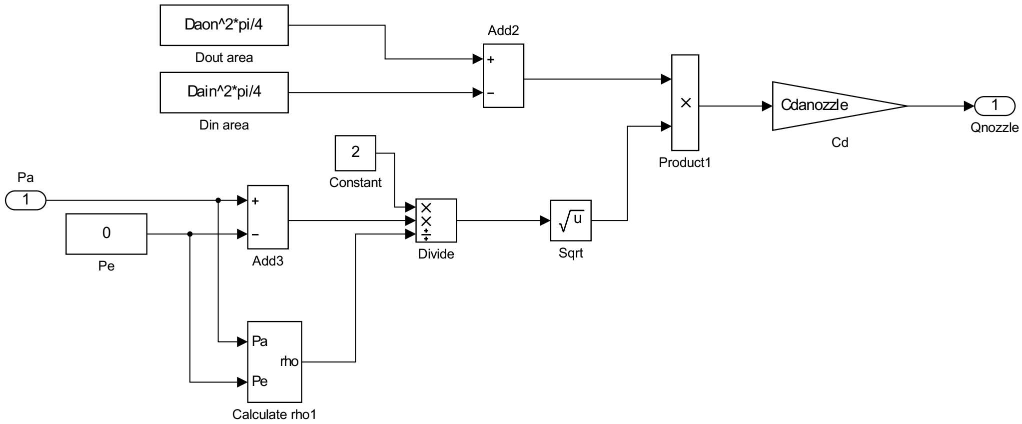

Figure 5.5. The Simulink model of the air nozzle.

The first verification is to see if the model produce similar result as measured data when the system is operating at normal conditions. This corresponds to a dutycycle of 38% on the airvalve and an air system pressure of 148 kPa. However as the flowmeter induces a 10 kPa pressure rise to the system, the system pressure is instead set to 158 kPa for the simulations. The simulation setup is given a constant air pressure from which it calculates a corresponding air outlet flow. The comparison between the simulated and measured values can be seen in figure 5.6.

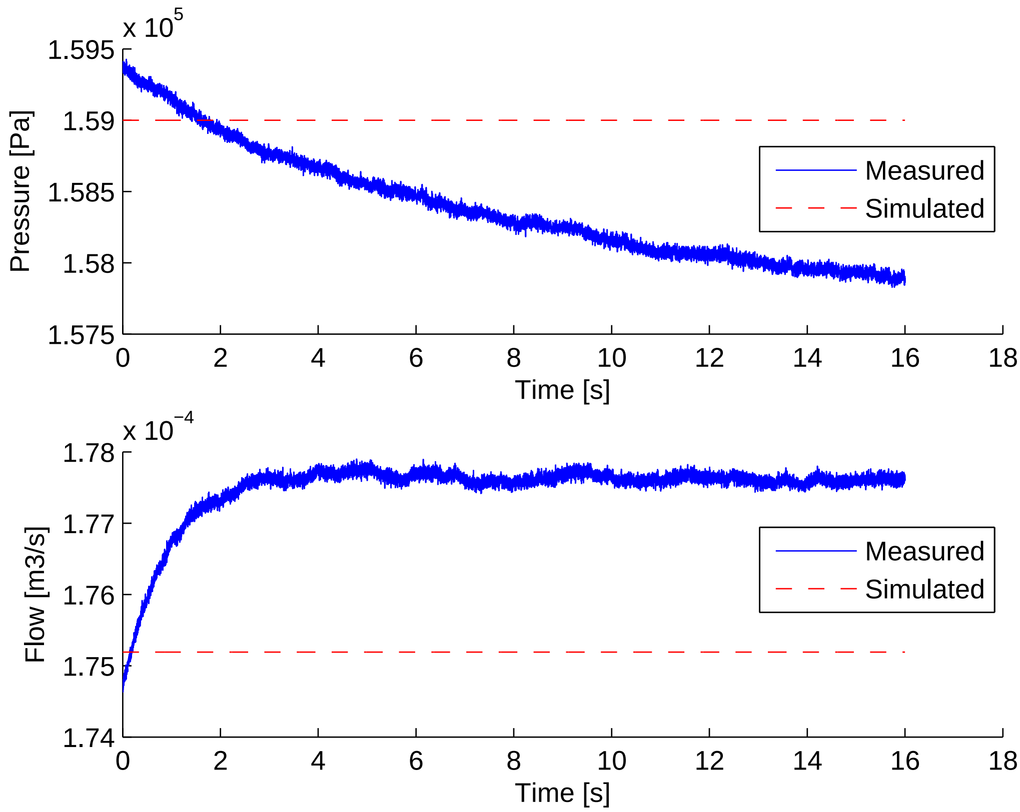

Figure 5.6. A plot that shows the measured and simulated pressure and outflow rate through air nozzle

As the plot shows the simulated value is close to the measured values, the deviation of the pressure is 0.6% and the deviation of flow is 2.13%, which is below the set goal and therefore acceptable.

The next test is shown in figure 5.7 and it is to see how the simulation deviate during the whole spectrum of pressure that the air nozzle operates at, from the atmospheric pressure up to 600 kPa. This is possible as there is no delay in the simulation, such as volumes that has to be filled before steady state is reached.

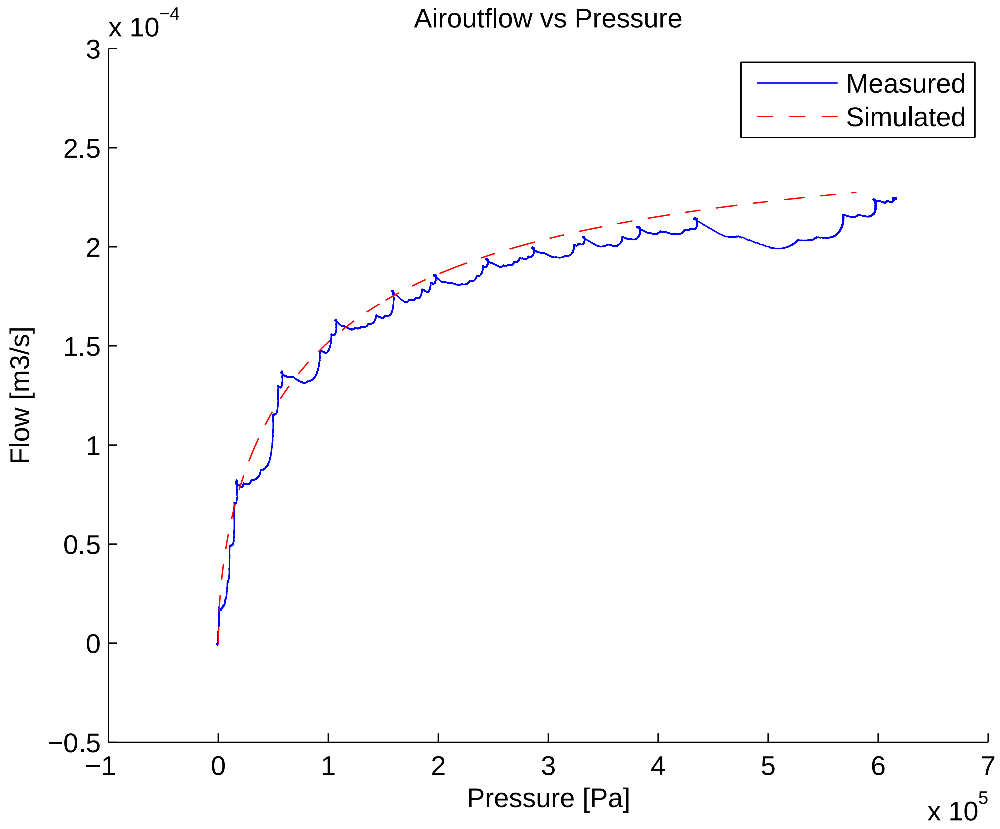

Figure 5.7. The measured and simulated outflow plotted with respect to pressure.

The simulated and measured data do match up very well for ideal condition and the deviation is always below the set goal. However, before the model can be accepted to be accurate enough, it has to be tested with disturbances in the system pressure. The next section will contain simulation where different physical parameters has been changed to increase the understanding of how changes to some of them effect the result.

5.2.1 Robustness of air nozzle model

The simulation at ideal conditions match up very well, unfortunately the conditions in reality is never ideal and it is therefore necessary to investigate how the model behaves when there is a disturbance in the input signal. The input disturbance that occurs at the air nozzle can be equated with a disturbance in the air canal pressure. The variation is simulated by adding an uniformed random number block in Simulink which has an amplitude of 0.1% of total pressure. The amplitude of the simulated disturbance is chosen to be as large as the measured disturbance. The simulation can be seen in figure 5.8.

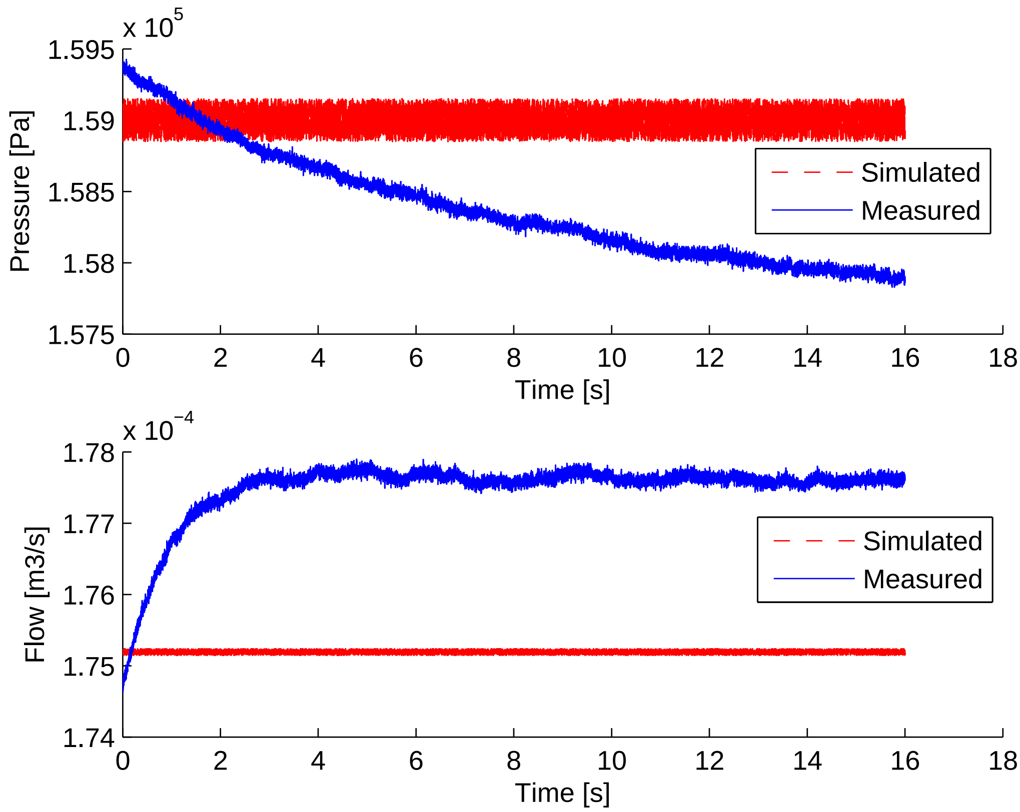

Figure 5.8. A simulation to show how the model handles disturbances at the input signal, the pressure disturbance is at 0.1% of total pressure.

The figure indicates that the model handles pressure disturbances very well. Even as the generated disturbance is larger than the measured pressure variation the simulated model gives a lower deviating outflow.

It is not only the operation condition that varies but the mechanical parts as well. Parts are not identical and it is important that the system can still operate even if its mechanical parts have a variation from the ideal one. For the next simulation physical parameters has been slightly modified as a try to capture how the system behaves over a wider range of conditions. First, the temperature is changed from 22°C to the specified lowest temperature the truck is suppose to operate in −40°C, as well as a slightly higher temperature 60°C. This is the temperature of the air in the system not the ambient temperature. The diameter of the orifice is also changed to see how the orifice deviation influence the result, a combined plot showing all simulation as well as the original is shown in figure 5.9.

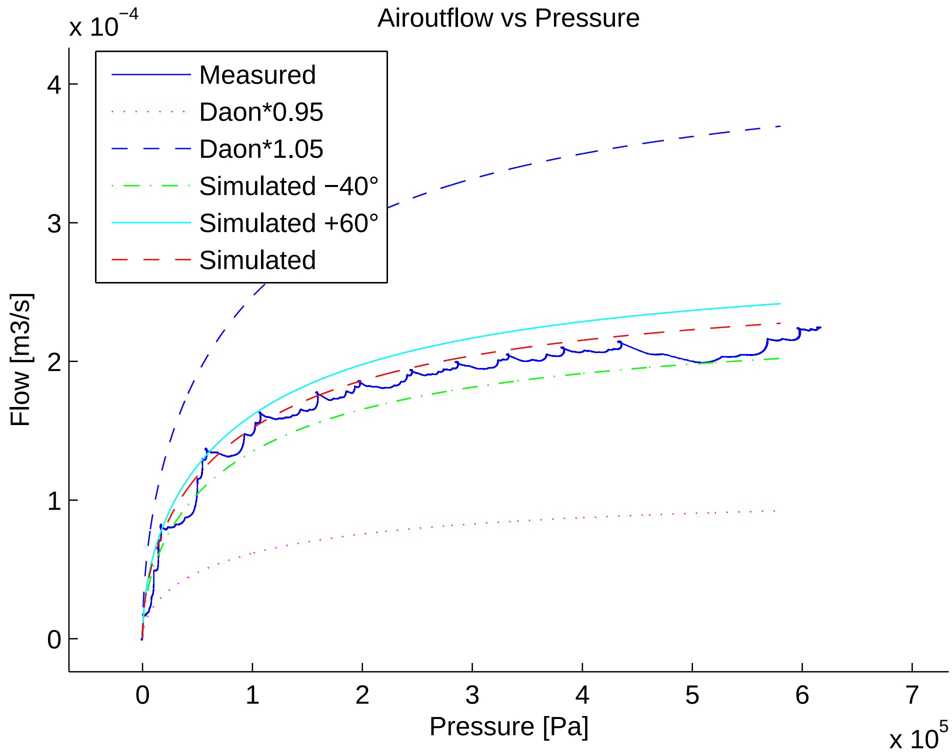

Figure 5.9. Illustrate the out flow difference at different pressure will change due to changes to physical parameters.

It can be concluded, from the simulations, that a change in temperature is not that crucial as the change corresponds to a deviation of $+6\%$ at $-40°$C and -11% at $+60°$C. However, a small change in the diameter of the orifice has a huge impact on the flow through. A diameter change of only $\pm5\%$ resulted in a deviation as large as $\pm60\%$, this shows that it is very important to keep the diameter of the orifice as close to the diameter that is determined during the development process as possible.

The air nozzle model does match the measured nozzle very well even when input disturbances is added to the system. The simulations also shows that the system is not very sensitive to the air temperature but a small change in diameter cause a huge impact on the flow. It is therefore necessary to maintain a good manufacturing process to keep the variation as small as possible among nozzles to keep the system from deviate as much.

5.3 Simulation and verification of urea nozzle

The urea nozzle is built on the same model as the air nozzle with different set of parameter values. Those parameters seen in table 5.2 are determined the same way as for the air nozzle.

Table 5.2. Fixed geometry parameters for urea nozzle

Symbol	Description	Value	Units
D_{out}	Outer diameter of the orifice	1	mm
T	Absolute temperature of the fluid	295	K
$R_{specific}$	Gas constant for air	287.058	J/Kg K
$C_{dunozzle}$	Discharge coefficient	0.5	n/a

At normal operation there will be no air flowing through urea nozzle which makes it pointless to test at normal operation. The simulation is instead tested at the second most used state, which is when the system opens the air valve to maximum to purge UWS from the urea canal. This state happens each time the engine is turned off. The comparison between the measured and simulated values is seen in figure 5.10.

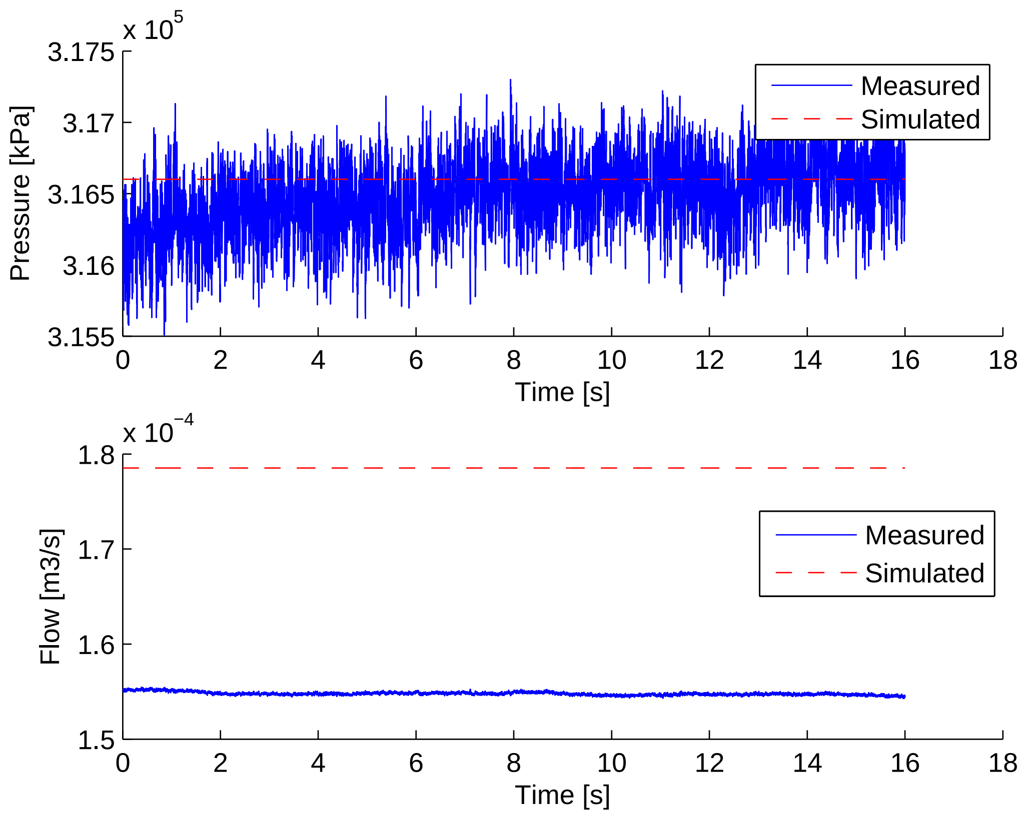

Figure 5.10. The measured and simulated value for max pressure in urea canal.

The figure shows that the model give 15% higher outlet flow for the same pressure, which is slightly higher then the set goal. To get a better understanding if the measured data deviate equal over all pressures a simulation over the complete pressure range is made, figure 5.11 presents the result from that simulation.

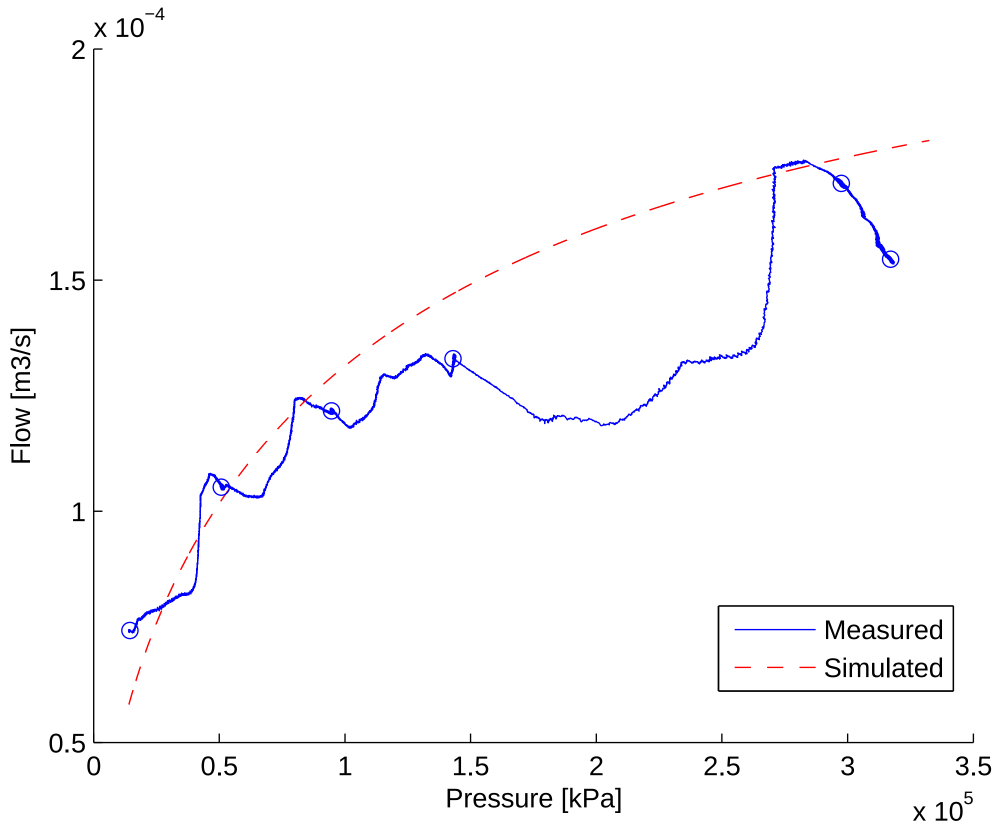

Figure 5.11. The measured and simulated flow rate with respect to pressure, the steady state pressure is marked with blue circles.

As the real system has volumes to fill only steady state pressure can be considered, in the figure those are marked with blue circles. Here it is seen that it is only the last circle that deviate as much as 15%, at other points the simulated and measured values is much closer to each other. A possible reason for this can be that the leakage in the system is not taken into account. Due to that the urea flow is not measured but computed from air inflow and outflow the leakage in the system is then included in the flow through the urea nozzle. The model assumes to cope with the target as most steady state points is within the limits.

5.3.1 Robustness of urea nozzle model

The procedure to investigate if the model is as robust as the real system is done in the same way as for the air nozzle. At first in steady state test, a disturbance in the urea pressure is induced with an amplitude of ±0.1 %, this is as large as the measured disturbance. The result from that simulation is shown in figure 5.12.

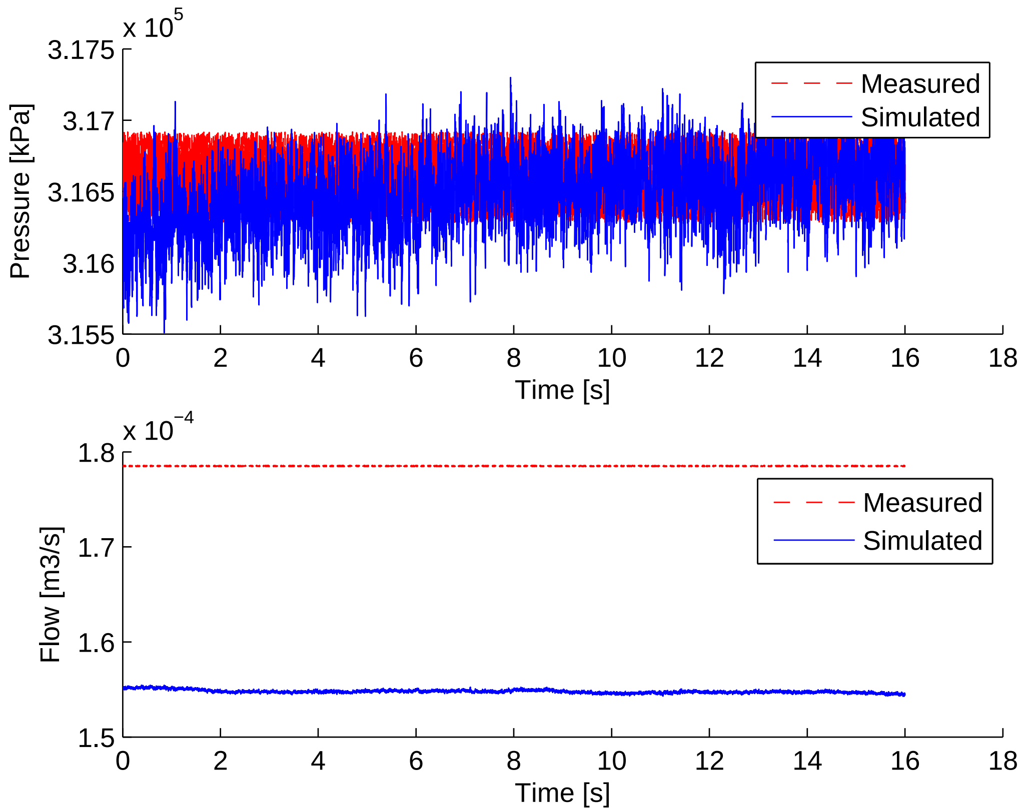

Figure 5.12. Illustration on how the simulated model behaves when there is a pressure disturbance.

From the figure it is seen that the difference at outlet flow at highest achieved pressure is still as high as without the disturbance. The test proves that the model is robust even though it is not a perfect model of the system. Further it is also tested with changes to the physical parameters as for the air nozzle to see how sensitive the model and real system is for physical deviation and the result is shown in figure 5.13.

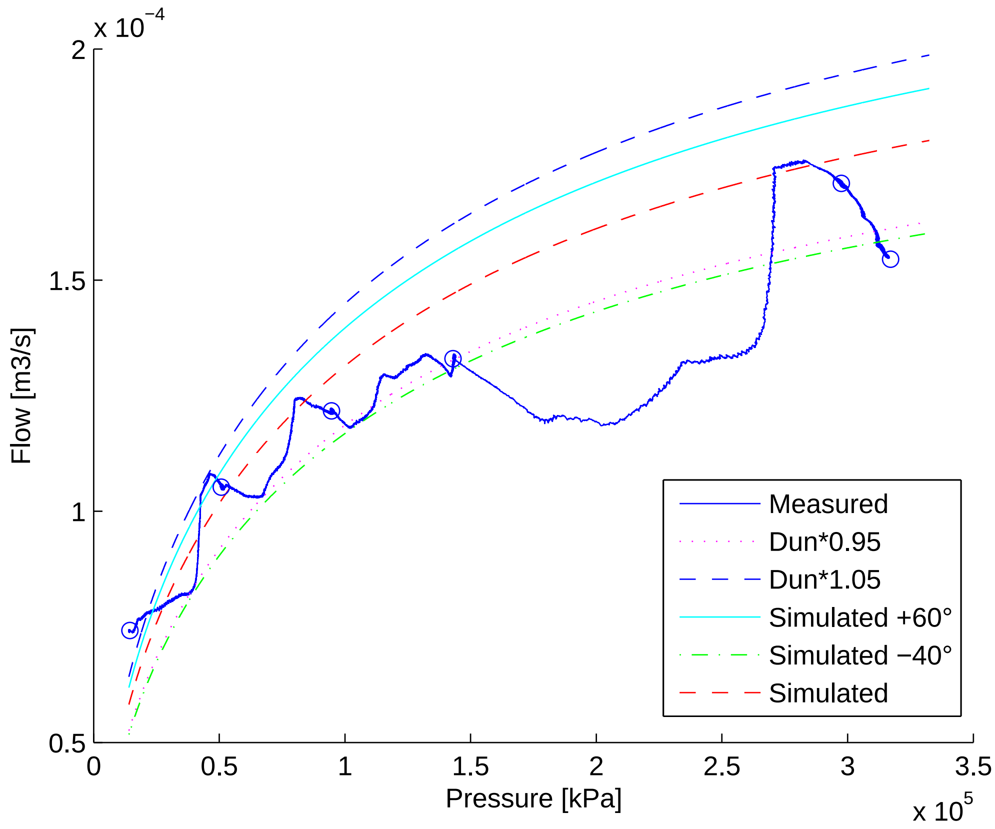

Figure 5.13. Shows how the urea outlet flow at different pressures changes with physical parameter variation.

To be able to relate to the air nozzle the deviation values are taken at 158 kPa. The deviation from the original simulation when changing the temperature is the same, $+6\%$ and -11%, as when the temperature is changed for the air nozzle. However, when the diameter is changed with the same percentage namely $\pm5\%$ it corresponds to a deviation from original simulation with $\pm10\%$. A reason for this is that the diameter for the urea nozzle is smaller than the air nozzle diameter. Thus the same percentage deviation corresponds to a smaller absolute deviation from its original diameter. Even though the nozzle is less sensitive for a deviation on the diameter then the air nozzle, it is still very sensitive for changes.

The urea nozzle is not as good as the air nozzle, but it still gives a good representation of the urea nozzle. It can handle input deviation and deviation to the physical parameters, well.

5.4 Simulation of pressure relief valve including air and urea nozzle

The parameter values that are shown in table 5.3 are derived by examination of existing hardware that has been used in a real installation. Due to the lack of measuring points in the real hardware it is not possible to only measure the pressure relief valve, the combined air/urea nozzle has to be included in the physical measuring.

Table 5.3. Fixed geometry parameters

Symbol	**Description**	**Value**	**Units**
D_c	Diameter on control volume 1	2.49	mm
k_c	Spring constant	0.3	N/mm
L_c	Length of control volume 1	2.87	mm
m_c	Mass of poppet and coil	0.11	g
θ_c	Cone angle of poppet	$\frac{\pi}{3}$	radians
C_{dc}	Discharge coefficient	0.8	none
β_a	Fluid bulk modulus	101	kPa
P_{diff}	Coulomb friction pressure	30	kPa
P_{cr}	Desired cracking pressure	290	kPa
Y_{max}	Maximum displacement of the poppet	3.6	mm
V_a	Air canal volume including hoses	9.15	dm^3
V_u	Urea canal volume including hoses	6	dm^3
T	Absolute temperature of the fluid	295	K
$R_{specific}$	Gas constant for air	287.058	J/Kg K

The Simulink model is seen in figure 5.14 and it is based on the governing equations derived in section 4.2. The subsystems in figure 5.14 can be seen in appendix B.

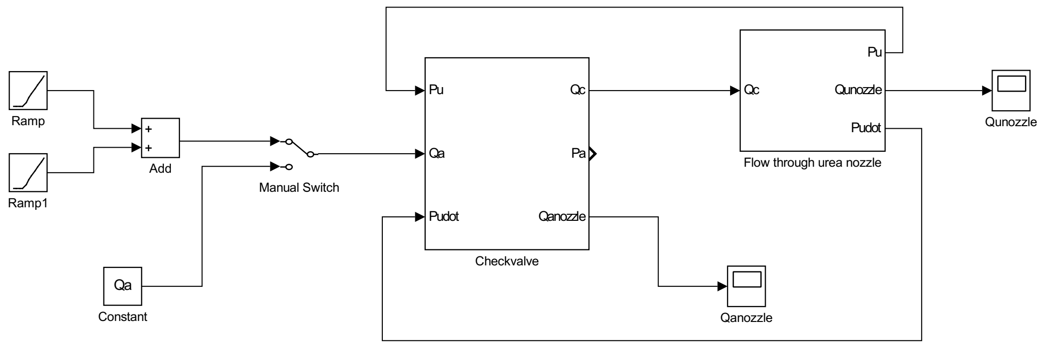

Figure 5.14. Simulink model of the model that is used to simulate the pressure relief valve.

This model takes flow into the air canal Q_a as input and compute the air pressure P_a, the flow through the pressure relief valve and air nozzle Q_c and $Q_{anozzle}$ respectively. The flow through the pressure relief valve is then used to calculate the pressure in the urea canal P_u that is used as input in urea nozzle block to compute the flow through urea nozzle $Q_{unozzle}$. The first step of verifying the model is by first looking at steady state for specific inflows Q_a, one where the pressure relief valve is closed and one where it is open. Then a step from one inflow to another is done to match the systems transient. Figure 5.15 illustrates the simulation result for the inflow when the dutycycle of the airvalve is equal to 38%.

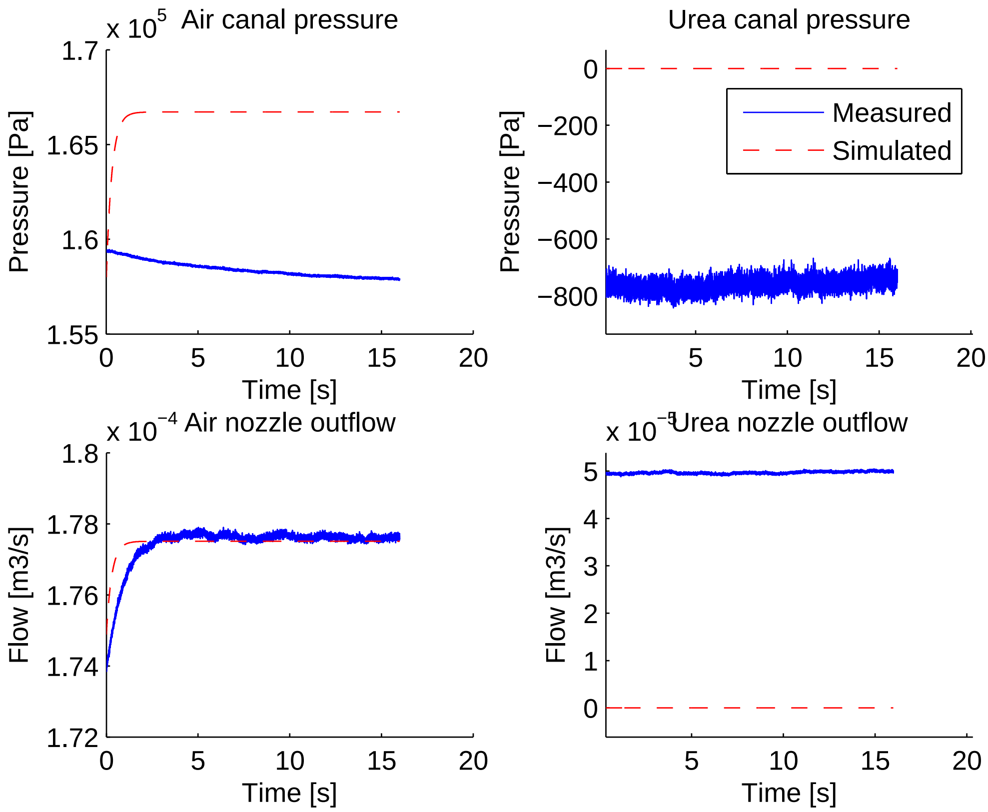

Figure 5.15. Shows the simulated and measured data for a 38% dutycycle, the pressure relief valve is not open.

It can be concluded from the figure that the air pressure and flow simulation values corresponds well with the measured values. The pressure difference is below 4%, while the flow out of the system match up close to an exact match of each others. Important to notice is that the pressure in the urea canal and flow out of it is not zero for the measured data even as the pressure in the air canal is well below the cracking pressure for the pressure relief valve. This is because of a leakage in the system that is included into the urea outflow. So the flow which is seen as the urea outlet flow in figure 5.15 is actually the leakage within the system. The measured pressure in the urea canal is negative, this is traced back to a small calibration difference in the measuring unit.

The next simulation is for a dutycycle which gives the maximum of air flow into the system, figure 5.16 shows the result of the simulation.

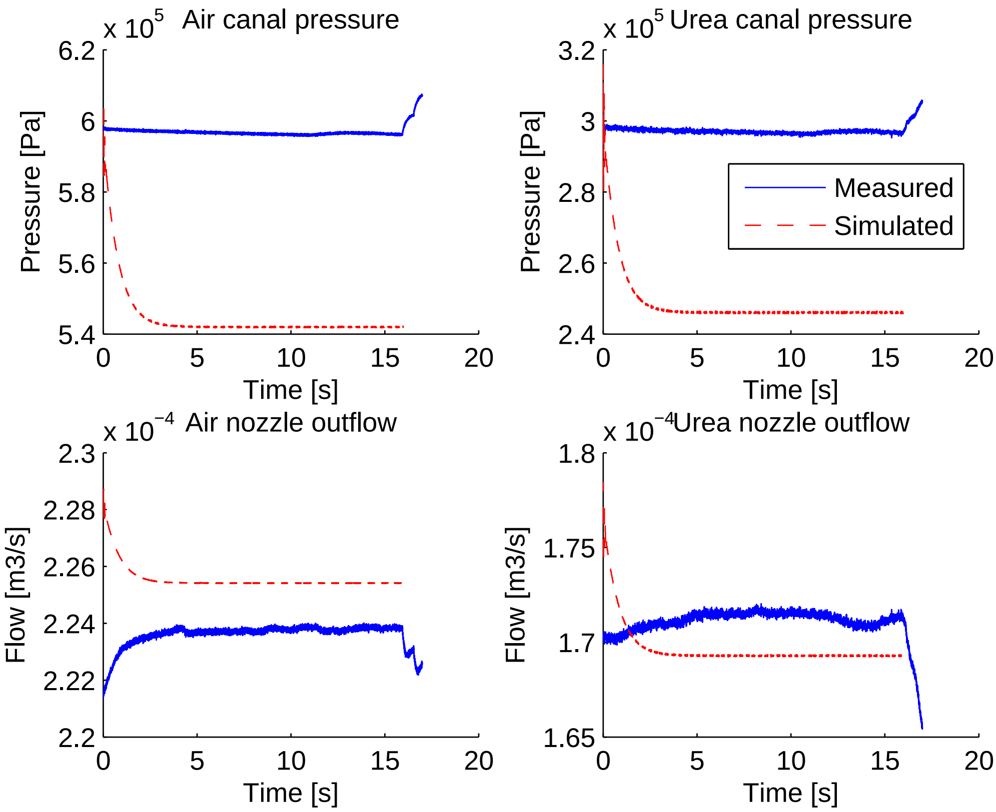

Figure 5.16. Plot of the simulated and measured data for a maximum open air valve equals to at least a 50% dutycycle, the pressure relief valve is open.

The difference here between simulation and measured data is slightly larger, the air pressure difference is 10% lower and the urea pressure difference is at 16% lower. This is a slightly higher deviation then what it should manage and it is due to the leakage within the system. As the leakage is not included in the model, the model compensates by giving a higher outflow which in the end result in a lower air canal pressure. Even though the urea canal pressure is 16% lower the outlet flow difference is only 1.3%.

It is not enough to only measure steady state points as they do not capture transient dynamics of the system. For the next simulation a dutycycle step of the air valve is simulated from 38-40%, this is shown in figure 5.17.

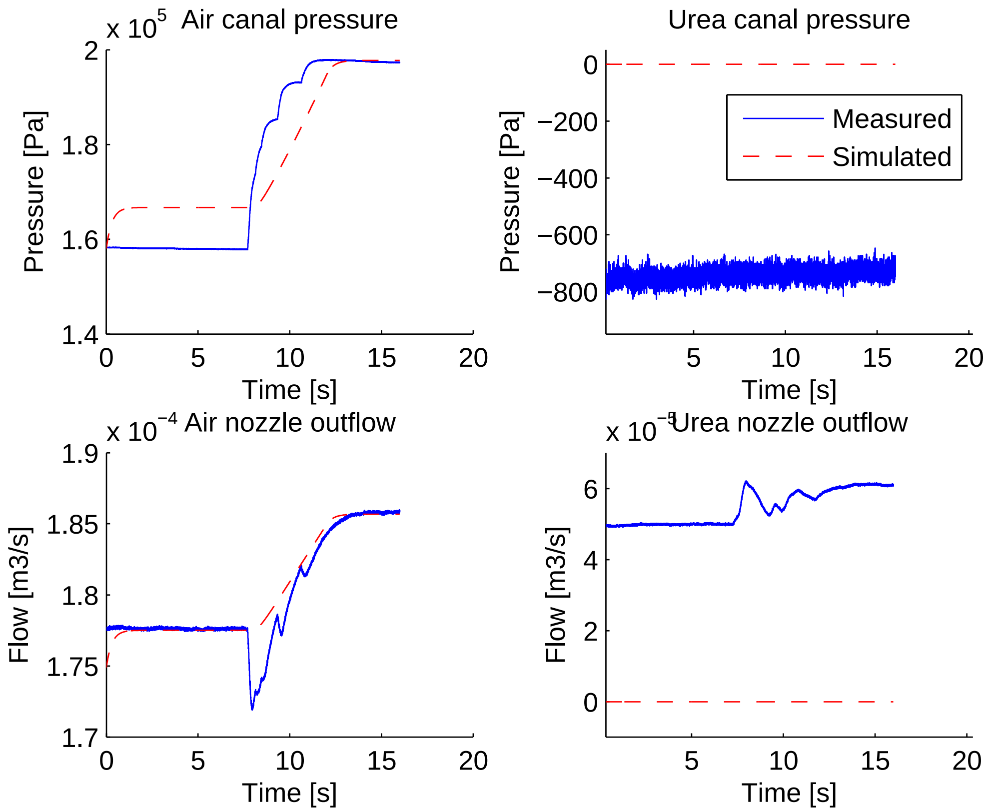

Figure 5.17. Plot of the simulated and measured data for a step from 38-40% dutycycle, to capture transients in the system.

The simulated transient and the measured transient of the system match each other very well. The simulated system is marginally slower then the measured system. The figure also shows that at the same moment as the dutycycle went from 38 to 40% the air outflow dropped. This flow drop can be a combination of the increased turbulence due to the quickly raised air canal pressure along with the urea outflow spike.

5.4.1 Robustness of pressure relief valve and nozzle model

The test of robustness is done by adding a disturbance to the inflow in order see how the pressure behaves. Figure 5.18 shows how the system behaves when there exist a disturbance on the flow into the system.

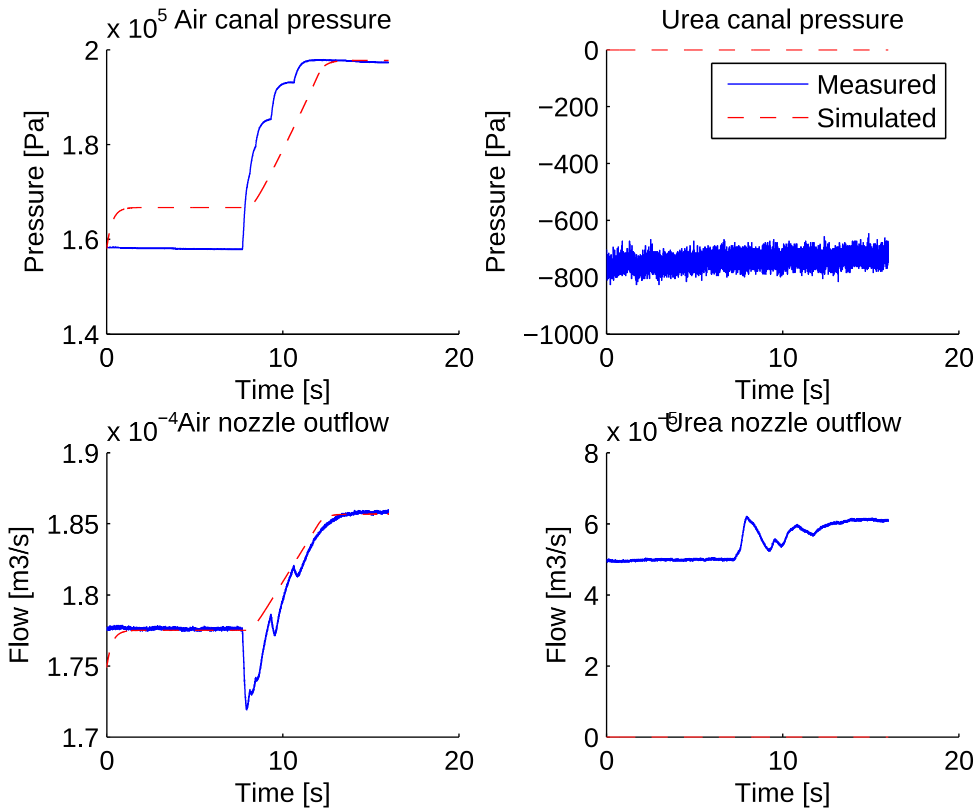

Figure 5.18. How the system behaves when there is a disturbance on the inflow.

The disturbance is chosen to be as large as for the measured data, which is at the measured pressure around $\pm 0.1\%$. There is little impact because of the disturbance.

The physical parameters that is changed for the next test is selected to prioritize changes in parameters which is more likely to be applied to the real system. The parameters that will be changed is the temperature and the spring constant. However, the spring constant is changed but the cracking pressure will still be the same, which means that the spring has to be less preloaded when the spring constant is higher and vice verse to achieve the same cracking pressure.

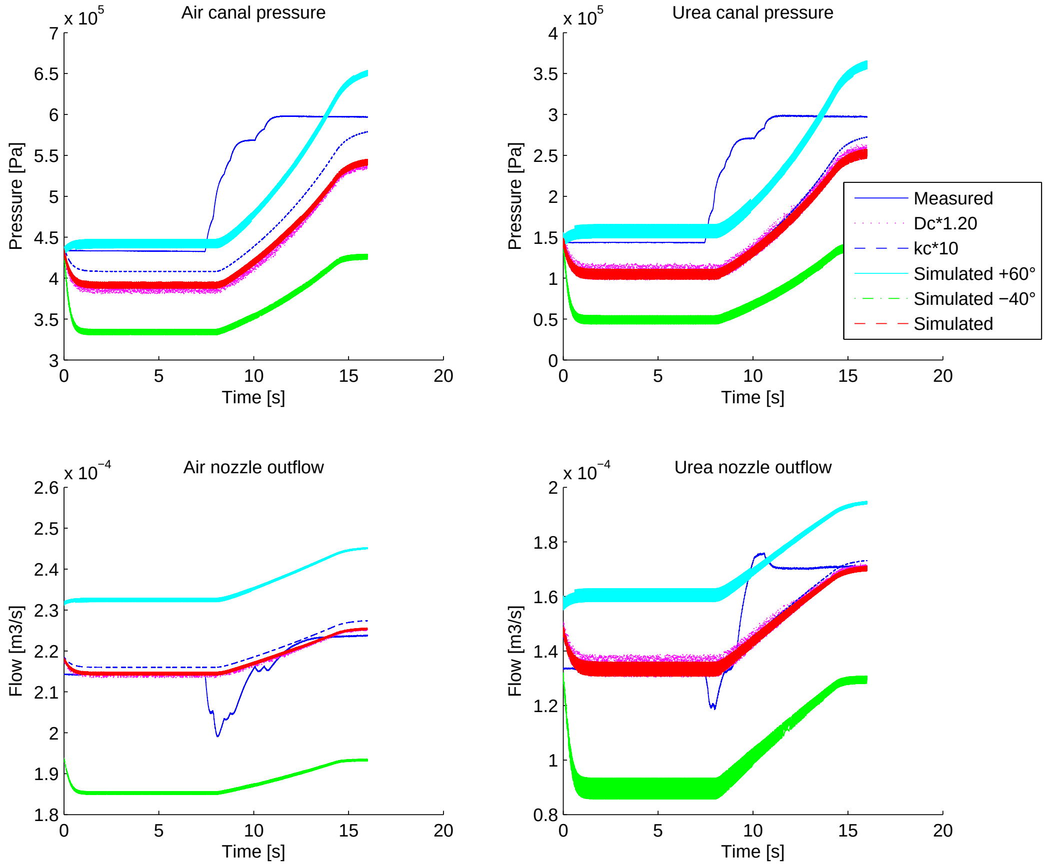

Figure 5.19. How variation of physical parameters affect the performance of the pressure relief valve and nozzle

The plot shows that a change in temperature makes a large impact on the system, part of the impact is due to that the in flow fed to the model is given in mass flow and when recalculated into a volumetric flow the temperature is used. A temperature of $-40°$C results in a 11% lower inflow giving a lower pressure in both canals.

The model matches the reality well even when disturbances is added to the inflow. The simulations indicates that the change of spring constant is not that crucial as long as the cracking pressure stays the same. It also shows that the air temperature does the same impact on the system pressure as for the nozzles.

5.5 Simulation of air valve

This section is to verify the air valve to see if the measured and simulated inflow match up for different dutycycles. The model takes a DC current that spans from 0 to 1 A, where it corresponds to the dutycycle percentage of the AC current.

The physical parameters seen in table 5.4, have been derived by measurements and the number of turns of the solenoid has been determined through the experiment seen in appendix A. The design parameter C_{da} have been determined through test iterations.

Table 5.4. Fixed geometry parameters for the air valve

Symbol	**Description**	**Value**	**Units**
D_a	Diameter on control volume 1	1.2	mm
L_a	Length of control volume 1	2.4	mm
k_a	Spring constant	2500	N/m
x_{pre}	Springs preload distance	0.68	mm
m_a	Mass of plunger	3.76	g
d	Diameter of the plunger	7.05	mm;
a	Length of the plunger	17.3	mm
θ_a	Cone angle of plunger	$\frac{\pi}{2}$	radians
C_{da}	Discharge coefficient	0.4	none
β	Fluid bulk modulus	142	kPa
μ_0	Permeability of free space	$4 * \pi * 10^{-7}$	N/A^2
μ_p	Permeability of the plunger	0.22	N/A^2
N	Number of turn of the solenoid	2500	turns
c	Thickness of guide tube	2	mm
x_{max}	Maximum displacement of the plunger	0.6	mm

The first is to see whether the simulation and measurements match up at normal operation steady state. Normal operation for the air valve is at a dutycycle of 38% and the result of that simulation can be seen in figure 5.6.

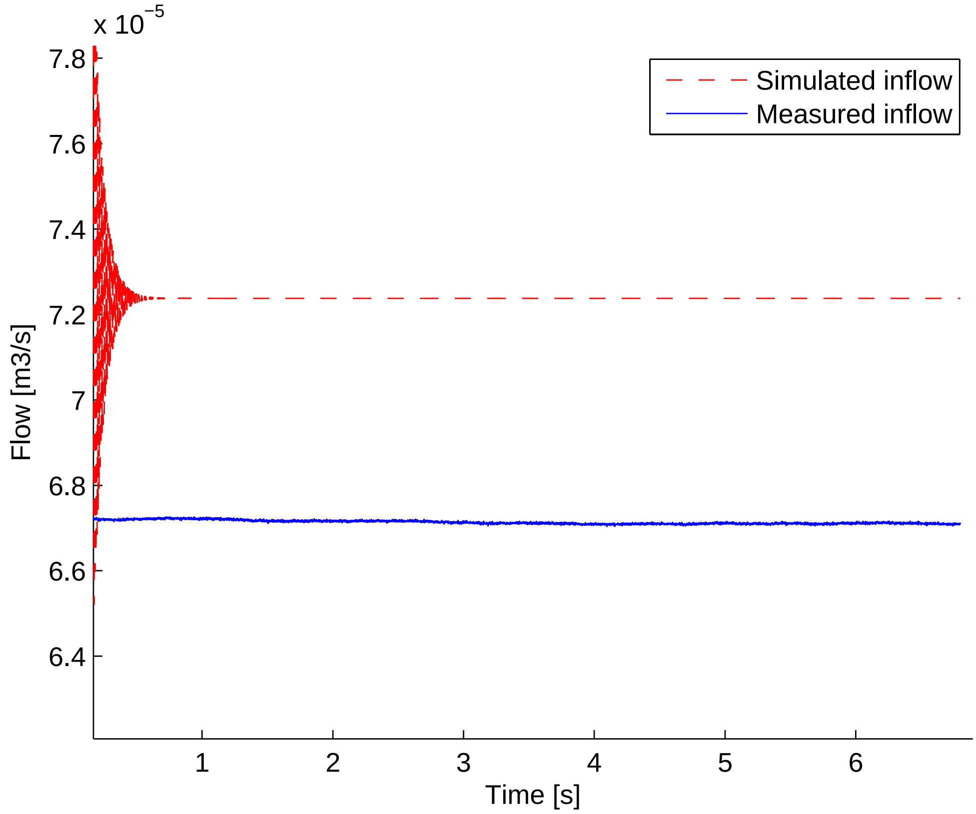

Figure 5.20. The measured and simulated flow through the air valve at 38% dutycycle.

From the figure it can be seen that the simulation match the measurements good, it deviates 8% from the measured data. The deviation is below the set goal even though the air valve is a complex system containing nonlinearities that have been approximated. It is therefore necessary to see how the simulation and measured data match up when the dutycycle is increased from 0 to 100%, the result is seen in figure 5.21.

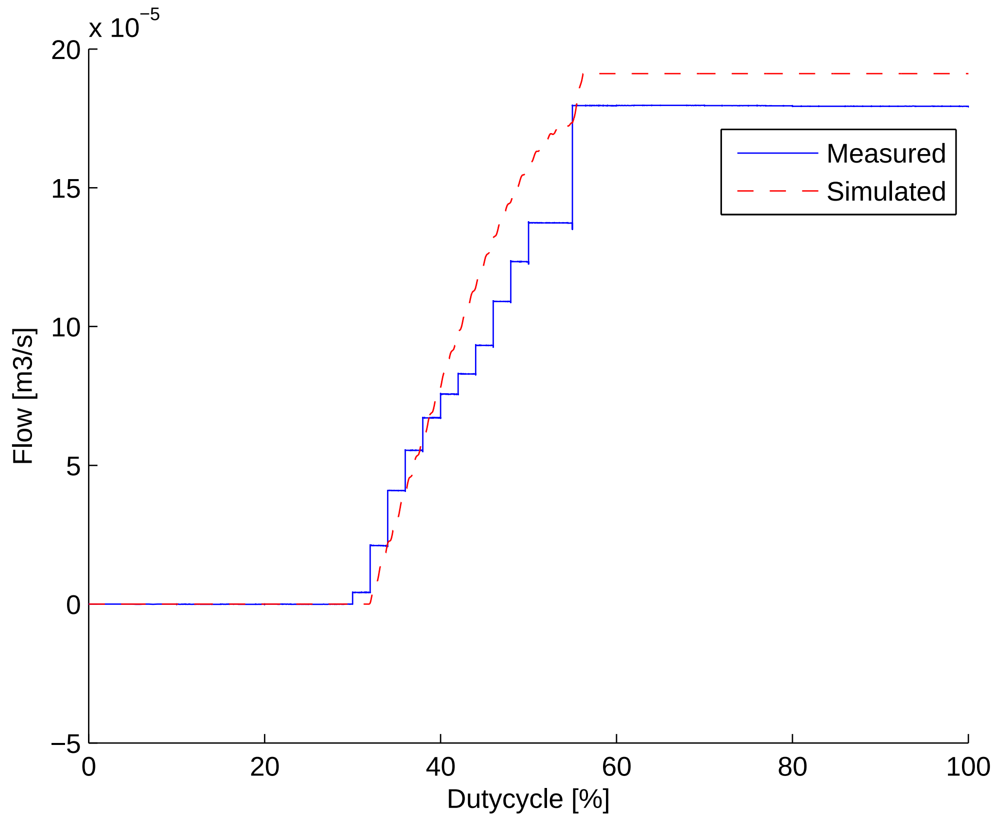

Figure 5.21. Measured and simulated inflow data plotted against dutycycle where it is increased from 0 to 100%.

From the figure it can be concluded that the simulated and measured data match up well even though they are slightly different from each other. A possible reason to why they are slightly different is that F_{mag} is computed by approximate the flux linkage as a function of the solenoid's inductance. To give a better model the curve fitting method might have been a better choice. The air valve manage the deviation goal due to the small variation in the two most used states, normal operation and when it is maximum open.

There is however a problem with the model as the measured inflow is in general one tenth of the outflow. The problem is assumed to be caused by how the density is calculated, the problem is discussed later in chapter 6.

5.6 Robustness of air valve

The air valve model will be tested with input disturbances to verify that the model can manage input disturbances as well. The input disturbance will be added to the inlet pressure to the air valve and the result is seen in figure 5.12.

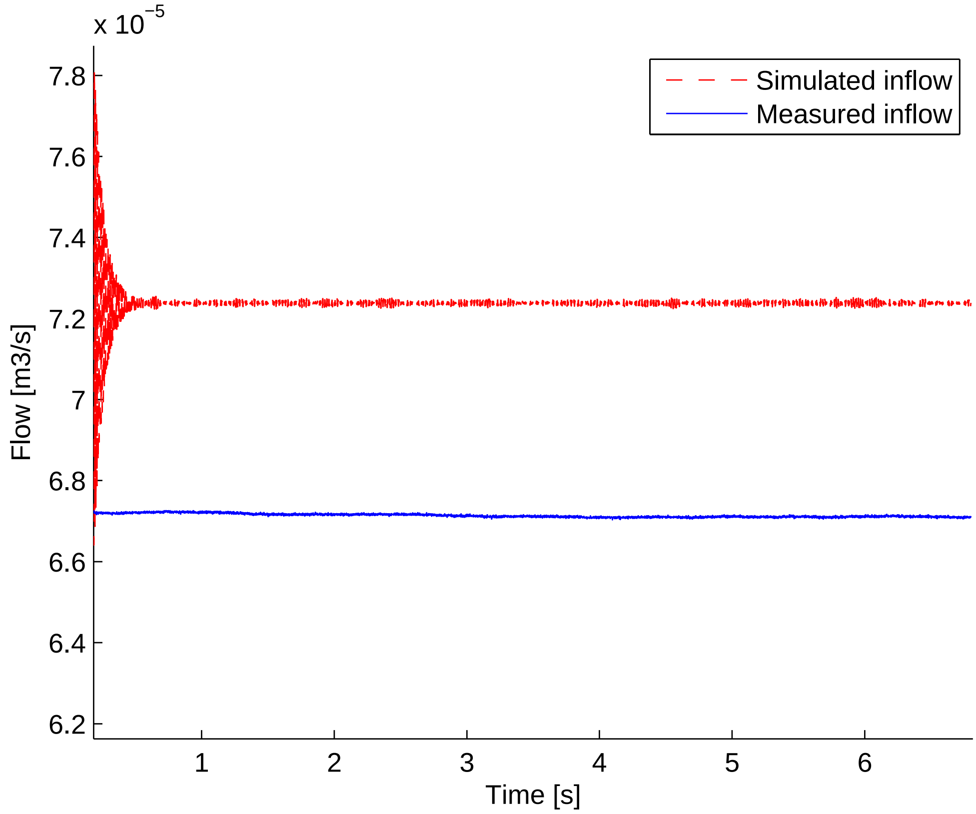

Figure 5.22. The figure show the simulated flow through the air valve when a disturbance to the inlet pressure is added that is equally large as for the measured pressure.

From the figure it can be concluded that the simulation can manage a disturbance to the inlet pressure equally good as the real system. The disturbance to the inlet pressure is measured to be 0.1% large.

The last simulation that will be shown is a simulation to see how parameter changes influence the flow through the air valve. The temperature will be changed from original to $-40°$C and to $60°$C. The second parameter that is changed is the number of turns of the solenoid to see how much it impact the air valve, the variation to number of turns is $\pm 5\%$. The result from the simulation is shown in figure 5.23.

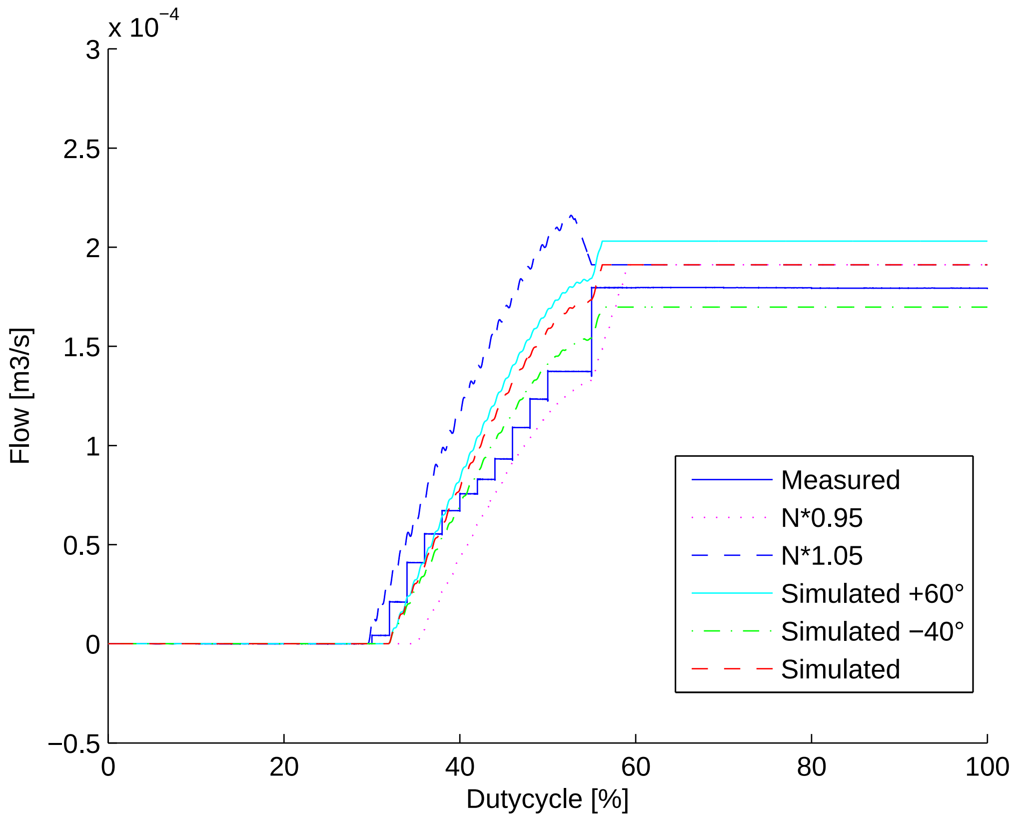

Figure 5.23. The figure show the simulated flow through the air valve for the different parameters changes.

The temperature induce +6 and −11% flow change at normal operation, precisely as for the air and urea nozzle. However, a variation to number of turns of the solenoid gives a larger impact to the flow through the air valve, at normal operation it gave 62% larger flow for the 5% increase and −56% lesser flow for the 5% decrease.

From the figures above it can be concluded that the model of the air valve is a good approximation of the real air valve. The model can handle input disturbances equally good as the real system. Since the model can handle the goals it is accepted as a valid model of the system.

6 Discussion

A problem that was encountered during the studies was how to compute the density. It was first encountered at late stages when the measurements of the real system was made. The flowmeter that measured the air flow did measured it in mass flow and the mathematical model used volumetric flow to calculate the pressure in the system. Until now the density that had been used was fixed even as the pressure ranged from atmospheric pressure up to 600 kPa and density of gases are greatly depending on pressure. As the topic being investigated it became even more complex as the simulation needed density at an orifice with different pressure on each side. The problem evolved from simply making the density change with pressure to an discussion of what pressure or combination of pressures that had to be used to calculate density. After thoroughly researching of theses and empirical studies on the model it was concluded that to compute the density of a gas that flows through an orifice with different pressure on each side the best match with measured data was when the mean absolute pressure was used.

However, this way of computing density resulted in that the volumetric inlet flow was a tenth of the volumetric outflow. It was still the best way to compute the density that had been encountered during the research and empirical testing of the system.

The leak-free constrain was disproved during measurements of the real system as seen in chapter 5. That made an impact on the urea nozzle outflow as it is computed from the measured air inflow/outflow. The included flow leakage deteriorated the models ability to match the measurements. However, could this be solved by measure the outlet flow to match the model with. By measure all inlet and outlet flow the leakage could be computed and then a leakage model could be made. This would increase the dynamics that the mathematical model could capture and also increase the usefulness of the model. The flowmeters that was available could only measure gas flow and was sensitive to liquids it was advised against measuring urea outlet flow. If more test were done, it would be handy to use a flowmeter that could measure urea outlet flow.

7 Conclusion

The model that has been derived in this thesis corresponds well to the real system as seen in chapter 5 and almost all models manage to meet the goals. The model that is closest to the real system is the air nozzle where the simulated and measured data correlate to each other very well. On the other hand, the urea nozzle model did not manage the goal at all pressures. The models maximum deviation is 15 % and that is at maximum pressure but otherwise it is within margins. The model for pressure relief valve and the air valve is a good enough approximation of the real system as well. The result of the pressure relief valve is negatively affected by the not so perfect model of urea nozzle. It is due to the chain reaction of a too high simulated urea nozzle outflow leading to a lower system pressure compared to the measured system. Regarding the model of the air valve it is as good as it can be when the magnetic force approximation. However, there is some minor influences that negatively affect the result, such as the neglected leakage in the system. The neglected leakage make a large impact at the urea nozzle as the urea outflow is computed indirectly from measured air inflow and air outflow and thus the leakage is included into the urea outlet flow. This results in that the measured urea outlet flow includes the leakage in the system, this is not ideal to match the real flow out of urea against the simulated values.

Future work on this topic is to make a model of the urea subsystem which then can be integrated with this model to get a model of the whole system. It is also important to further investigate the density and how it shall be computed. It may also be useful to investigate how much better the curve fitting technique of approximating the magnetic force of the solenoid. It may be worth the additional computational complexity to increase how well it matches the reality.

Bibliography

[1] DieselNet. *Gaseous Emissions*;. [Accessed 4st of September, 2014]. [Online]. Available from: http://dieselnet.com/tech/emi_gas.php.

[2] Agency EE. *Nitrogen oxides (NOx) emissions (APE 002) - Assessment published Jan 2014*;. [Accessed 10st of September, 2014]. [Online]. Available from: http://www.eea.europa.eu/data-and-maps/indicators/eea-32-nitrogen-oxides-nox-emissions-1/assessment.2010-08-19.0140149032-3\#methodology.

[3] DieselNet. *What Are Diesel Emissions*;. [Accessed 16st of Januari, 2015]. [Online]. Available from: http://dieselnet.com/tech/emi_intro.php.

[4] DieselNet. *Emissions standards in European Union for heavy-duty trucks and bus engines*;. [Accessed: 4st of september, 2014]. [Online]. Avaliable from: https://www.dieselnet.com/standards/eu/hd.php.

[5] Nitin P. *EATS EPD SCHOOL 2012*. GTT Powertrain;. Report number: 1, 2012.

[6] Ireståhl D;. Test engineer consultant on GTT Powertrain. Personal communication. 2014-10.

[7] Birkhold F, Meingast U, Wassermann P, Deutschmann O. Analysis of the Injection of Urea-water-solution for automotive SCR DeNOx-Systems: Modeling of Two-phase Flow and Spray/Wall-Interaction, In:. *SAE Technical Paper*, 2006, doi:104271/2006-01-0643;.

[8] Åberg L. *Technical requirement, urea dosing system, installation requirement*. GTT Powertrain;. Report number: 08, 2013.

[9] Anderson Jr JD. Governing Equations of Fluid Dynamics. In: Wendt JF (eds.) *Computational Fluid Dynamics*. 3rd ed. Springer Verlag;. [Accessed: 10th of October, 2014]. [Online]. Available from: http://www.springer.com/cda/content/document/cda_downloaddocument/9783540850557-c1.pdf?SGWID=0-0-45-621403-p173839306.

[10] Computational Fluid Dynamics Modeling: Governing Equations. In: ASM International. 1990;.

[11] McDonough JM. *LECTURES IN ELEMENTARY FLUID DYNAMICS*. Departments of Mechanical Engineering and Mathematics University of Kentucky, Lexington;. [Accessed: 2014-10-10]. [Online]. Avaliable from: http://www.engr.uky.edu/~acfd/me330-lctrs.pdf.

[12] Pramås M. *Urea dosing system*. GTT Powertrain;. Report number: 05, 2013.

[13] Stone JA. Discharge Coefficients and Steady-State Flow Forces for Hydraulic Poppet Valves. *ASME Journal of Basic Engineering.* (1960);82(144-154):1041–1048.

[14] Love J. Flow: Orifices. In: *Process Automation Handbook.* 1th ed. Springer London;. [Accessed: 15th of October, 2014]. [Online]. Available from: http://dx.doi.org/10.1007/978-1-84628-282-9_12.

[15] Theodore L. Chapter 5 - Gas Laws. In: *Heat Transfer Applications for the Practicing Engineer.* Hoboken NJ, USA. John Wiley and Sons. Press: 2011. p15-51;.

[16] Pfeiffer F. *Dynamics and stability issues of poppet type pressure relief valves.* University of Missouri; (2004).

[17] Jurić Z, Kulenović Z, Kulenović D. Influence Of The Hydraulic Relief Valve Poppet Geometry On Valve Performance. In:*14th International Research/Expert Conference "Trends in the Development of Machinery and Associated Technology" TMT 2010, Mediterranean Cruise.* (2010);p. 517–520.

[18] Cheung NC, Lim KW, Rahman MF. *Modelling a linear and limited travel solenoid.* University of New South Wales; (1993).

[19] Lunge SP, Kurode S, Chhibber B. Proportional Actuator from On Off Solenoid Valve using Sliding Modes. In: *Proceedings of the 1st International and 16th National Conference on Machines and Mechanisms (iNaCoMM2013)*; (2013). p. 1020–1027.

[20] Meisel J. *Solenoid (electricity)*;. [Accessed 11st of December, 2014]. [Online]. Available from: http://www.accessscience.com/content/solenoid-electricity/634200.

[21] Sheng-Nian C, Hai-Yang L, Cheng-Tao X, Bao-Lin P. Proportional Solenoid Valve Flow Hysteresis Modeling Based on PSO Algorithm. In: *Instrumentation, Measurement, Computer, Communication and Control (IMCCC)*; 2013. p. 1064–1067.

[22] David W Spitzer PE. *How Pressure Variations Affect Flow Measurement*;. [Accessed 11st of Januari, 2015]. [Online]. Available from: http://www.flowcontrolnetwork.com/articles/how-pressure-variations-affect-flow-measurement.

Appendix A

Experiment to determine number of turns of the coil

This appendix will describe how to determine the number of turns of a solenoid where no data of the solenoid is known, the derivation begins from the equation of inductance in a solenoid:

$$L = \mu_0 \mu \frac{N^2 * A_s}{l} \tag{A.1}$$

By rearrange the terms and solve the equation for N instead the following equation is achieved:

$$N = \sqrt{\frac{Ll}{\mu_0 \mu A_c}} \tag{A.2}$$

Here is l the length of the coil, A_c is the cross-sectional area of the coil, μ_0 is the magnetic constant in free space and the solenoids inductance will be determined by the following experiment.

To experimentally determine the inductance of a black box solenoid is made with use of a DC power unit, the solenoid, an ammeter and an oscilloscope. The power unit is connected to the solenoid and the solenoid is connected to the power unit and thus forming a closed loop circuit. The input to the oscilloscope is given from the ammeter which enclosed the input current to the solenoid, a schematic view of the setup can be seen in figure A.1. To get the experiment to be as close to reality as possible the current which is feed through the solenoid is a pulse width modulated (PWM) signal which is generated from the ACM with a frequency of 800 Hz and a voltage of 28 V. The generated dutycycle on the PWM signal will be changed to match the dutycycle that is commonly in normal operation. The measured parameters is the used in the following equation to compute the solenoids inductance:

$$L = \frac{V * t}{I_s} = \frac{V_p}{f * I_s} \tag{A.3}$$

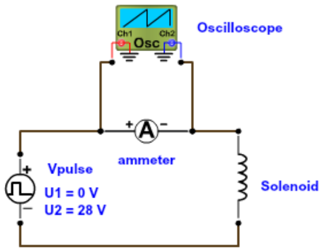

Figure A.1. A schematic view of how the experiment to determine the inductance L of the coil was setup.

Where V_p is the voltage peak which the power unit is generating, f is the frequency in which the PWM signal is modulated at and I_s is the measured current on the input to the solenoid this is given by the ammeter. In the table below the parameter values is presented at different dutycycles and with or without the solenoid plunger also the calculated inductance and the number of turn of the solenoid calculated using A.3 and A.2 is presented in table A.1.

Table A.1. Measured parametric values and calculated number of turn of the solenoid

	With core				Without core			
Duty cycle [%]	10	30	40	50	10	30	40	50
Peak voltage [V]	28	28	28	28	28	28	28	28
Frequency [Hz]	800	800	800	800	800	800	800	800
Peak current [A]	0.6268	0.7036	0.7157	0.7744	0.6428	0.7349	0.7668	0.8100
Inductance [H]	0.0558	0.0497	0.0489	0.0452	0.0545	0.0476	0.0456	0.0432
Number of turns	2707	2555	2534	2446	2674	2500	2448	2382

Appendix B

Simulink model

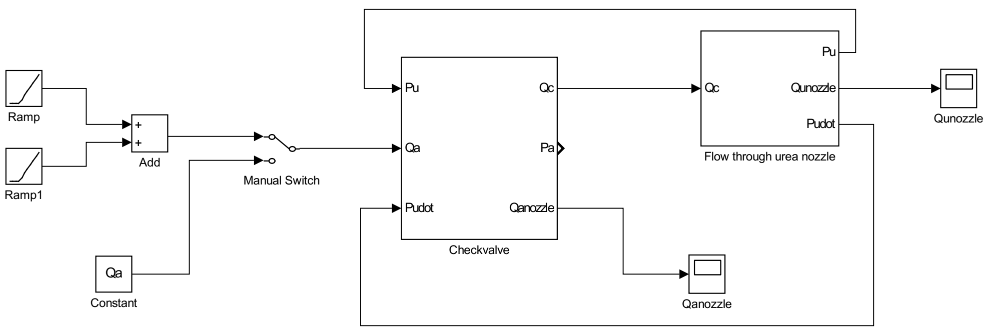

Figure B.1. Overview of the whole Simulink model.

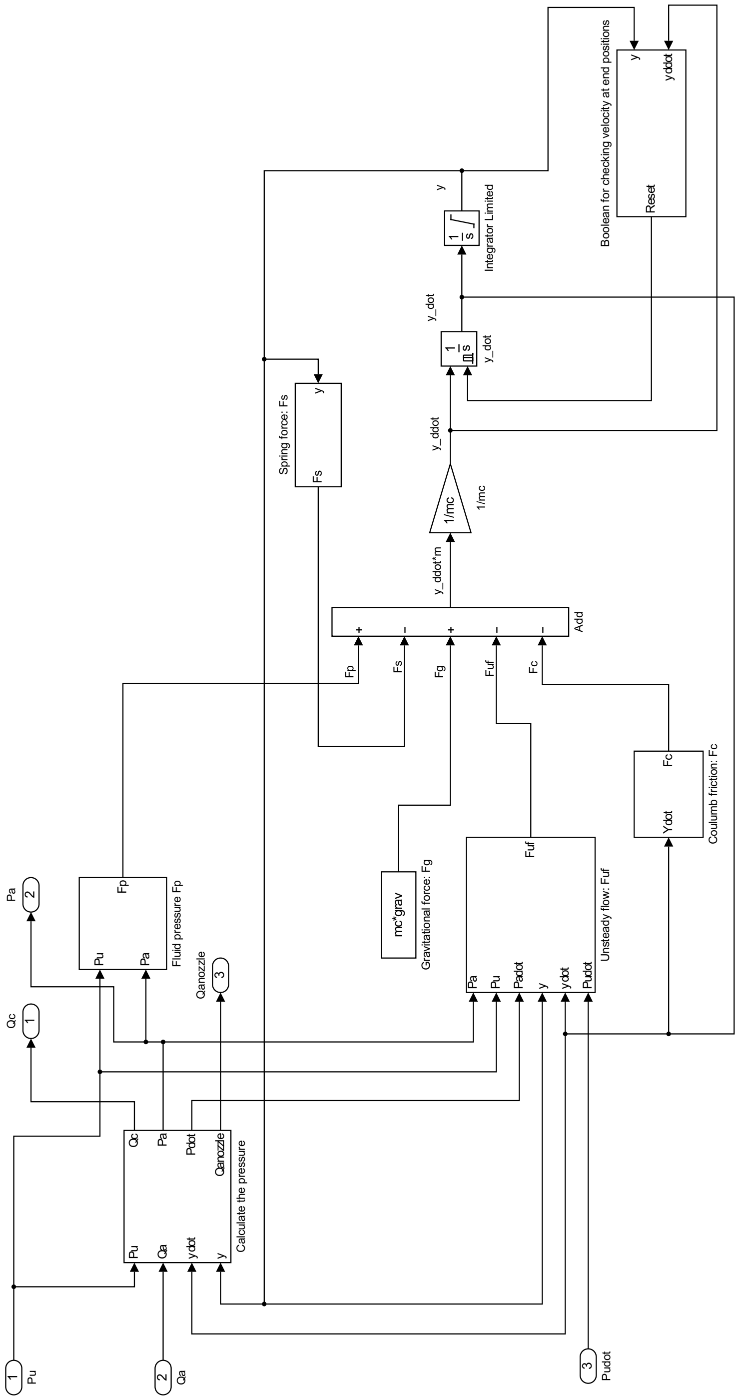

Figure B.2. Overview of the Simulink model of the checkvalve.

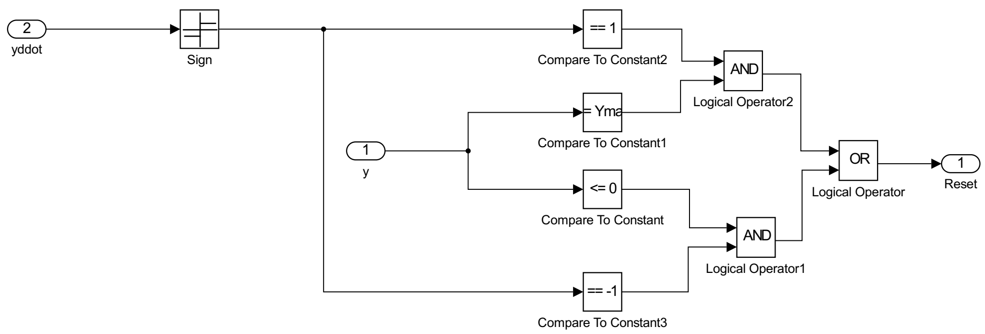

Figure B.3. Overview of the Simulink model of the reset velocity integration logic.

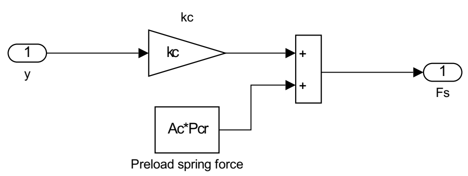

Figure B.4. Overview of the Simulink model of the spring model.

Figure B.5. Overview of the Simulink model of Coulombs friction.

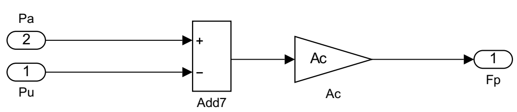

Figure B.6. Overview of the Simulink model of the fluid pressure force.

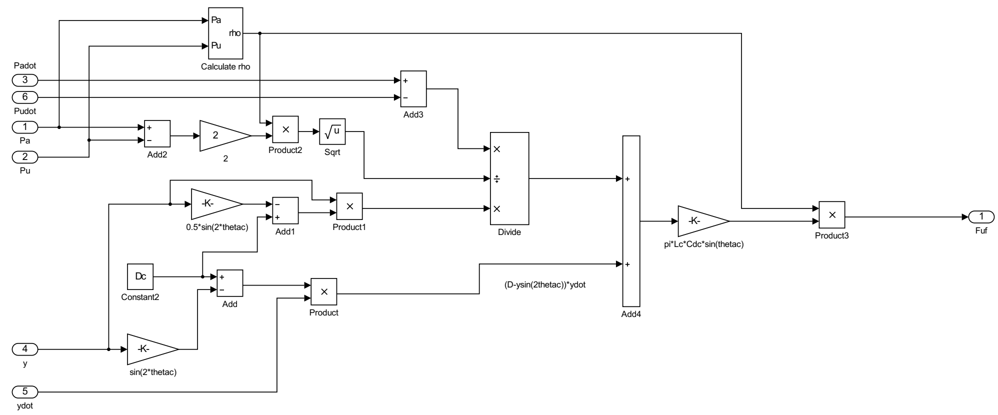

Figure B.7. Overview of the Simulink model of the unsteady flow force.

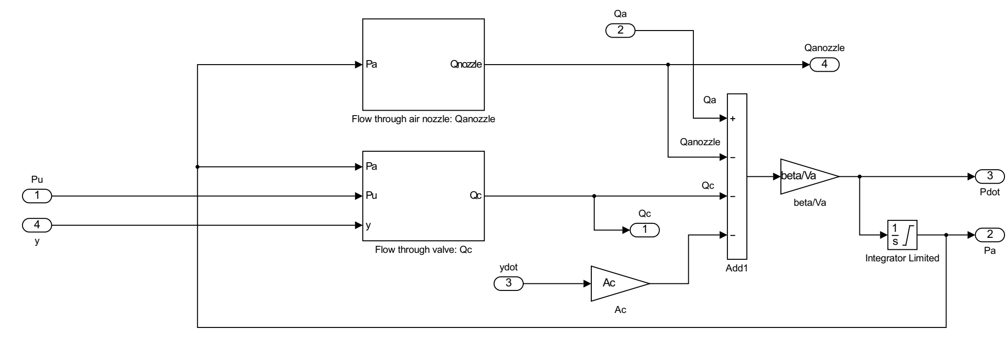

Figure B.8. Overview of the Simulink model of the air canal model.

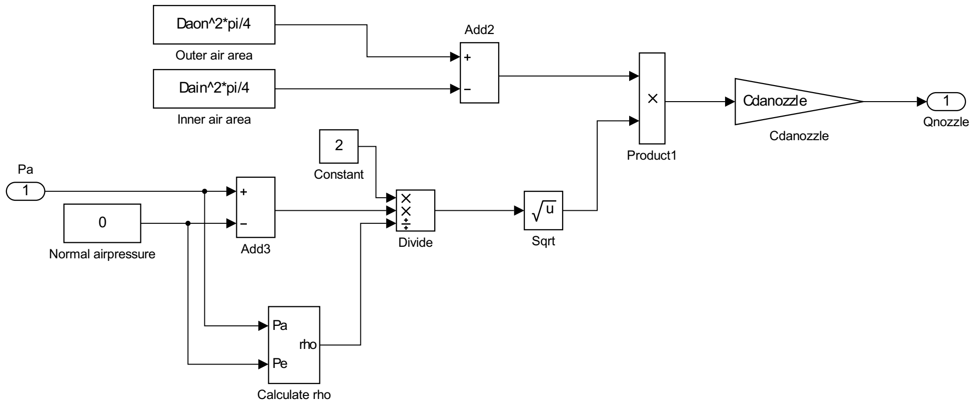

Figure B.9. Overview of the Simulink model of the flow through the air nozzle.

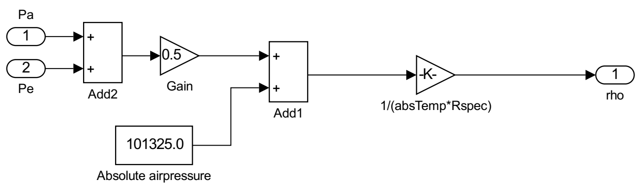

Figure B.10. Overview of the Simulink model of the density model.

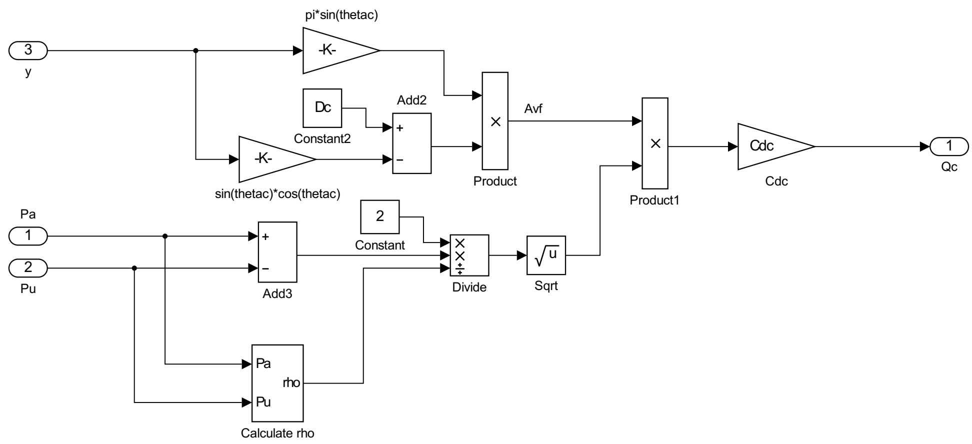

Figure B.11. Overview of the Simulink model of the flow through the pressure relief valve.

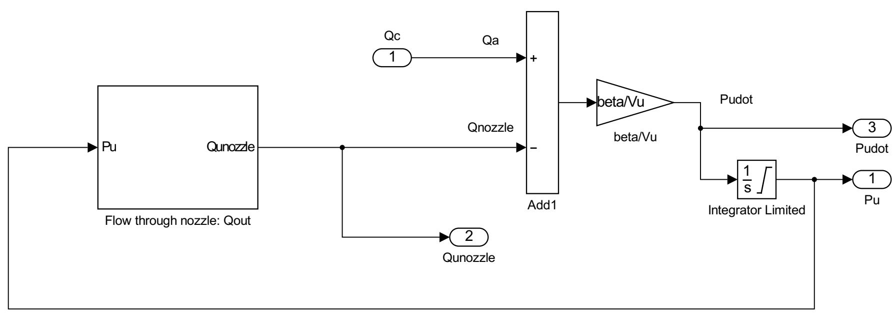

Figure B.12. Overview of the Simulink model of the urea canal model.

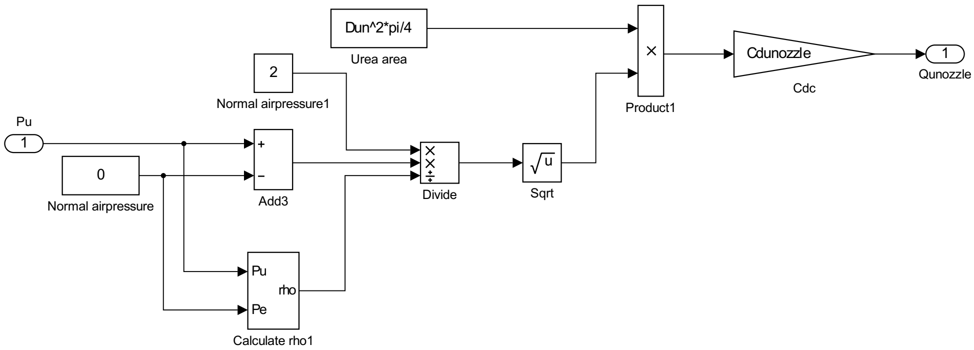

Figure B.13. Overview of the Simulink model of the flow through the urea nozzle.

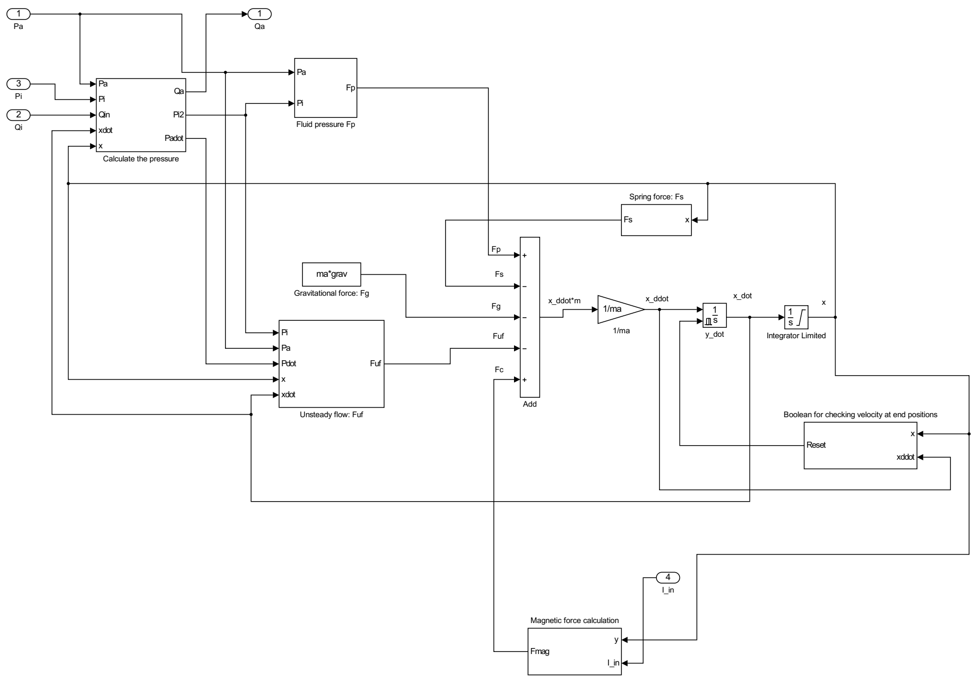

Figure B.14. Overview of the Simulink model of the air valve.

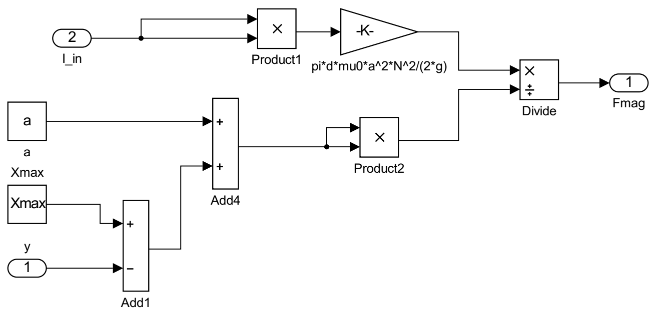

Figure B.15. Overview of the Simulink model of the magnetic force.

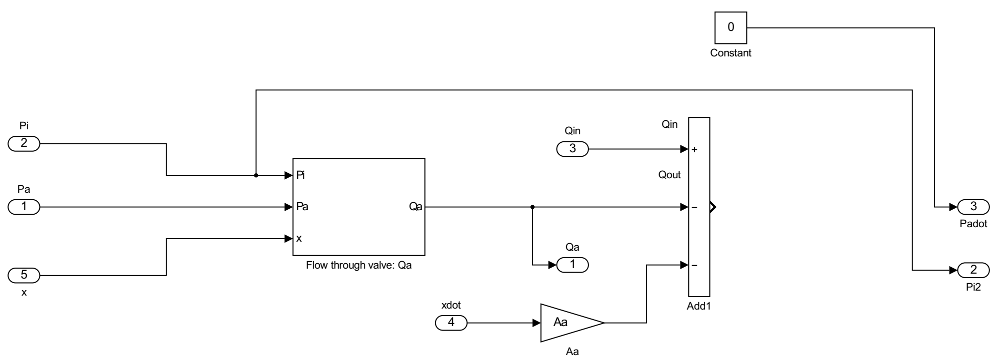

Figure B.16. Overview of the Simulink model of the pressure rise equation of the air valve.